

Detection of NaCl Ions and TNF- α Cytokines using Pyroelectric Effect in Liquid-Silicon Heterostructures

by
Yupeng Zhao

A Thesis Submitted in Partial Fulfillment of the Requirements for the Degree of
Bachelor of Applied Science

in the
School of Engineering Science

© Yupeng Zhao 2023
SIMON FRASER UNIVERSITY
Fall 2023

Copyright in this work is held by the author. Please ensure that any reproduction
or re-use is done in accordance with the relevant national copyright legislation.

APPROVAL

Name: Yupeng Zhao

Degree: Bachelor of Applied Science Honours

Title of Thesis: Detection of NaCl Ions and TNF-alpha Cytokines using Pyroelectric Effect in Liquid-Silicon Heterostructures

Dr. Cheng Li, P.Eng.
Director, School of Engineering Science

Examining Committee:

Dr. Michael Adachi, P.Eng.
Professor, School of Engineering Science

Dr. Ash Parameswaran, P.Eng.
Professor, School of Engineering Science

Dr. Majid Shokoufi, P.Eng.
Professor, School of Engineering Science

Date Approved: Dec. 14th, 2023

Abstract

The change of electric properties at a liquid-solid interface due to solution concentration variation has the potential to contribute toward the design of a concentration sensor. This study investigates the pyroelectric and photoelectric properties at a liquid-semiconductor heterojunction for NaCl ion and TNF- α cytokine detection. The concentration sensor is constructed by utilizing the LED-triggered pyroelectric and photoelectric effects. Two experimental stages involve NaCl solution characterization using bare n-type silicon and TNF- α cytokine solution detection using aptamer-functionalized silicon. The collected electric current responses aim to establish the determination of solution concentrations down to nanomolar for NaCl (aq.) and nanomolar to femtomolar for TNF- α . The research methodology encompasses detailed materials and methods, including circuit designs and key component selections for the sensor prototype. Results reveal distinct electric current response levels correlating with solution concentrations, providing a foundation for the biosensor's efficacy. The biosensor prototype is encapsulated in a 3D-printed casing for accessibility. It demonstrates an integration of diverse components and shows promising results of detecting NaCl (aq.) concentration down to micromolar and the potential of pushing the range down to nanomolar. The study also highlights the possibilities for future investigations, particularly in the systematic variation of the response measurement at the cytokine-aptamer interface and the refinement of the device construction.

Acknowledgments

I want to express my gratitude to all those who have contributed to the completion of this thesis. I am thankful for the invaluable guidance and support I have received from my supervisor, Dr. Michael Adachi, throughout the research process. My appreciation extends to the research group members, Ribwar Ahmadi, Amin Abnavi, and Hamidreza Ghanbari, for allowing me to shadow them during experiments to gain experience with procedures. Ribwar showed me the basic setup and routine for making electric signal measurements at a liquid-solid interface. Amin showed me the procedure for making a PDMS device. Hamidreza guided me through the process of silicon functionalization and cytokine protein solution preparation. All have been instrumental in shaping the direction and quality of this work.

A special note of appreciation goes to SFU Engineering and the NSERC for providing financial support through the Undergraduate Student Research Awards. This funding has been crucial to facilitating experiments and developing prototypes.

I thank my family and friends for their unwavering encouragement throughout this academic year. Their support has been a constant source of inspiration.

Table of Contents

Abstract	- 1 -
Acknowledgments	- 2 -
List of Figures	- 5 -
List of Tables	- 6 -
Chapter 1: Introduction	- 7 -
1.1 Rationale for the Study: Pyroelectric and Photoelectric Effects at Liquid-solid Heterojunctions ...	- 8 -
1.2 Thesis Structure	- 8 -
Chapter 2: Literature review	- 9 -
2.1 State of the Art of Biosensors Related to TNF- α Cytokine Detection and Current Devices' Limitations	- 9 -
2.2 State of the Art of NaCl (aq.) Concentration Detection and Corresponding Limitations	- 10 -
Chapter 3: Materials and Methods	- 11 -
3.1 LED as Pyroelectric and Photoelectric Effects' Triggering Source	- 11 -
3.2 Solution Preparation	- 11 -
3.3 Substrate Preparation	- 12 -
3.3.1 Silicon for NaCl (aq.).....	- 12 -
3.3.2 Aptamer Functionalization on Silicon with an Oxide Layer for Cytokine Solution	- 12 -
3.4 Constraining the Liquid-solid Interface Area with PDMS.....	- 13 -
3.5 Experiment Setup.....	- 14 -
3.6 Methods of Electrical Signal Measurement	- 15 -
3.7 Biosensor Prototype Design and Assembly	- 16 -
3.7.1 Circuit Design	- 16 -
3.7.2 Programming Design	- 18 -
3.7.3 Casing Design.....	- 20 -
3.8 Notes on Cleaning Procedures	- 21 -
3.8.1 Cleaning During an Experiment	- 21 -
3.8.2 Cleaning After an Experiment.....	- 21 -
Chapter 4: Results	- 23 -
4.1 Pyroelectric and Photoelectric Responses observed using a Source Meter	- 23 -
4.2 NaCl (aq.) on Silicon, Pyroelectric and Photoelectric Responses observed using an Oscilloscope-	24
-	-
4.3 NaCl (aq.) on Silicon, Pyroelectric and Photoelectric Responses Observed using the Biosensor Box	-
26 -	-

4.4 Capacitance Measurement at the NaCl (aq.)-silicon Interface.....	- 28 -
4.5 TNF- α Cytokine on Aptamer-functionalized Silicon, Pyroelectric and Photoelectric Responses Observed using an Oscilloscope	- 29 -
Chapter 5: Discussion, Conclusion, and Future Work	- 31 -
5.1 NaCl (aq.) Concentration Sensing	- 31 -
5.2 TNF- α Cytokine Concentration Sensing and Future Works	- 33 -
References	- 34 -
Appendix A: NaCl Solution Preparation	- 37 -
Appendix B: TNF-α Cytokine Protein Solution Preparation	- 38 -
Appendix C: Aptamer-Functionalization on an N-type Silicon Substrate with 5 nm of Aluminum Oxide Coating.....	- 39 -
Appendix D: PDMS Mixing, Degassing, and Baking	- 41 -
Appendix E: List of Biosensor Box PCB Component Footprints.....	- 42 -
Appendix F: Biosensor PCB Front and Back Copper Layers, and PCB Printing Specification....	- 43 -
Appendix G: List of 3D-printed Parts, Projection views, and Dimensions.....	- 44 -
Appendix H: Tables of Collected Data	- 56 -

List of Figures

Figure 1. Silicon substrate with surface features for interface area definition and solid probe contact: 3D drawing (left) and sample substrate (right).	- 12 -
Figure 2. Functionalized silicon substrate shined by a blue laser: picture taken without the filter (left) and with the filter (right).	- 13 -
Figure 3. Drawings of PDMS device mold: side piece (left) and bottom piece (right).	- 13 -
Figure 4. PDMS square well: 3D drawings (left) and baked device (right).	- 14 -
Figure 5. PDMS square well mounted on a silicon substrate using tape.	- 14 -
Figure 6. Schematic diagram for pyroelectric and photoelectric current generation.	- 14 -
Figure 7. Pyroelectric and photoelectric current measurement setup: positioning the contact probes.	- 15 -
Figure 8. Schematic block diagrams of circuits used for three signal measuring methods: (a) using a source meter. (b) using an oscilloscope, and (c) using an ADC.	- 15 -
Figure 9. Biosensor box circuit schematic diagram.	- 17 -
Figure 10. Breadboard implementation of the biosensor box circuit with probes.	- 18 -
Figure 11. PCB design, front (left) and back (right).	- 18 -
Figure 12. Program flowchart for customized ADC and data post-processing.	- 19 -
Figure 13. Biosensor casing parts: (a) Base piece, (b) substrate holder, (c) lid, (d) liquid probe support, (e) solid probe support, (f) LED holder, (g) square stand 32-0, (h) square stand 4-0, and (i) square washer 0-5.	- 20 -
Figure 14. Assembled biosensor box: (a) front, (b) right, and (c) isometric.	- 21 -
Figure 15. Current readings collected from a Keithley source meter subjected to 100 mM NaCl (aq.) on silicon.	- 23 -
Figure 16. Voltage readings collected from a Tektronix oscilloscope with NaCl solution concentrations at 2 pM, 200 pM, 20 nM, 20 μM, 1 mM, and 100 mM.	- 24 -
Figure 17. The oscilloscope readings of the current generated at the NaCl (aq.)-silicon interface due to pyroelectric and photoelectric effects: (a) transient response peak values, and (b) steady-state values. The legend on the side indicates the LED wavelength in nm followed by the intensity in mW/cm ² (e.g. 470, 13.4 is the 470 nm blue LED at 13.4 mW/cm ²).	- 26 -
Figure 18. Transient response peak values at the NaCl (aq.)-silicon interface measured using the biosensor box with voltage biases applied in series, including (a) reverse biases up to -0.4 V, and (b) forward biases up to 0.4 V. The legend on the side labels the biasing values.	- 28 -
Figure 19. Capacitance measurement at the liquid-solid interface plotted as the ratio against the 0-molar interface capacitance in blue. The transient current peak values collected at 0 bias are also plotted as ratios in red for pattern comparison.	- 29 -
Figure 20. Current response values over cytokine solution concentration at the liquid-solid interface between TNF-α cytokine solution and aptamer-functionalized silicon substrate, showing both (a) transient peaks and (b) steady-state values.	- 30 -
Figure 21. Front copper layer (left) and back copper layer (right).	- 43 -

List of Tables

Table 1. LED candidates.....	- 11 -
Table 2. Reverse bias voltages and their corresponding device sensitivity from 1 μM to 100 mM	- 28 -
Table 3. Forward bias voltages and their corresponding device sensitivity from 1 μM to 100 mM	- 28 -
Table 4. NaCl solution dilution ratios.	- 37 -
Table 5. TNF- α solution dilution ratios.	- 38 -
Table 6. Biosensor Box PCB component footprints.	- 42 -
Table 7. PCB printing specifications.....	- 43 -
Table 8. NaCl (aq.)-silicon interface transient peak currents at three wavelengths and two intensities due to pyroelectric and photoelectric effects, collected using the Tektronix oscilloscope.	- 56 -
Table 9. NaCl (aq.)-silicon interface steady-state currents.	- 56 -
Table 10. NaCl (aq.)-silicon interface transient peak currents due to pyroelectric and photoelectric effects with reverse voltage biases, collected using the biosensor box.	- 57 -
Table 11. NaCl (aq.)-silicon interface transient peak currents with forward voltage biases.	- 57 -
Table 12. NaCl (aq.)-silicon interface capacitance.	- 58 -
Table 13. TNF- α cytokine-aptamer interface electric current responses due to pyroelectric and photoelectric effects, collected using the Tektronix oscilloscope.	- 58 -

Chapter 1: Introduction

Tumor necrosis factor- α (TNF- α) plays a crucial role in the immune system and inflammation [1-3]. It is a cytokine classified under the TNF superfamily [1-3]. As a signaling molecule produced primarily by macrophages, TNF- α is involved in various pathological processes, including immune response, inflammation, apoptosis, and septic shock [1, 2]. While TNF- α concentration levels in the human body vary significantly depending on the disease and its severity, monitoring the concentration can help assess disease progression and guide treatment decisions [3, 4, 5].

This paper documents the research around constructing a TNF- α biosensor for concentration detection based on the pyroelectric and photoelectric responses at the liquid-solid interface [6, 7]. By observing the electric transient and steady-state responses triggered due to an external source, each solution concentration is mapped to an electric current value. Reversing the relation between the electric response and the solution concentration may provide a way of predicting the level of a solution concentration, which may lead to a low-cost method of detecting TNF- α .

The TNF- α cytokine solution concentration investigated in this paper ranges from femtomolar to nanomolar. Damas et al. showed that TNF- α concentration increases significantly among patients with septic shock, for instance [8]. Normal values for the concentration are 75 ± 15 pg/mL (4.3 pM), and the TNF- α serum level for the investigated patients ranged from 100 pg/mL (5.8 pM) to 5000 pg/mL (290 pM) [8]. Patients' median was 250 pg/mL (14.5 pM) [8]. The proposed femtomolar to nanomolar range of operation covers a broader scale than the concentration variations listed for septic shock, which could be potentially applicable to other inflammatory diseases.

Before diving into the investigation using TNF- α cytokine solutions and TNF- α aptamer-functionalized silicon substrates, the electric response data is collected using sodium chloride (NaCl) solutions against n-type silicon substrates. The detection of NaCl ions holds importance in industrial and scientific applications, driving the need for accurate measurement techniques. One primary application is in the field of corrosion prevention. The presence of NaCl ions in environments is a major contributor to corrosion on metallic surfaces [9]. Effective corrosion prevention strategies require precise monitoring of NaCl concentrations since elevated levels can accelerate corrosion processes [10, 11].

Unlike protein substances that decay over time, NaCl and silicon are easy to prepare and store. These substituting materials will help with providing insights into the electric response and concentration relation. The NaCl (aq.) concentration ranges from picomolar to millimolar. This range is selected such that it is wide enough to test the sensitivity and generate patterns for electric response. It does not go into the femtomolar region due to the high mobility of sodium ions, which leads to doubting the ions' presence in a highly diluted solution.

1.1 Rationale for the Study: Pyroelectric and Photoelectric Effects at Liquid-solid Heterojunctions

The pyroelectric effect occurs when charge carriers are generated within a material due to changes in temperature over time [12]. It is unlike the thermoelectric effect, where charge carriers move in response to a temperature gradient, or changes in temperature over space [13]. The pyroelectric effect is observed in materials possessing polar symmetry [12-14]. The electric dipoles in the material bulk react to temperature changes by a change of spontaneous polarization, which leads to a charge redistribution that generates an electric field [12, 13]. Such an electric field induces polar structures in the semiconductor substrate and leads to pyroelectric responses [14].

The photoelectric effect has been well-known over the past decades due to the wide applications of solar cells. It is a phenomenon in which materials emit electrons from their surfaces when exposed to electromagnetic radiation [15, 16]. When photons interact with the material, they transfer their energy to electrons, dislodging them from the surface [15, 16]. The energy carried by a photon is directly related to its frequency. If this energy surpasses the material's work function, electrons are liberated, and the remaining energy from the photon becomes the kinetic energy of the freed electron. [15, 16]. In the case of semiconductors, the band gap determines the minimum energy required for a striking photon to produce a charge.

Investigation of the two electric effects at an interface can proceed simultaneously. The pyroelectric effect responds to temperature changes, and the response stabilizes as the temperature settles. In contrast, the photoelectric effect responds to the presence of an incident light wave. Having a light source shining on the interface will produce a steady-state response. Combining the two will elevate the transient peak by the steady-state value due to the superposition of the responses.

1.2 Thesis Structure

The thesis laid out in the following chapters consists of a literature review, a specification of materials and methods, the results collected through experiments, a discussion reflecting each data set, and a conclusion summarizing the key findings. Throughout the thesis, detailed descriptions, figures, and tables are used to enhance the clarity of the presented information. Audiences may refer to the appendices for procedure recipes when rigorous methods are skipped in the thesis body for information flow. With this structured approach, this thesis aims to provide a comprehensive understanding of the construction and performance of the sensory device based on pyroelectric and photoelectric properties at a liquid-semiconductor heterojunction.

Chapter 2: Literature review

Chapter 2 presents a brief review of the existing literature concerning TNF- α solution concentration detection and NaCl (aq.) concentration detection. Also, it justifies the proposed approach based on the underlying principles of pyroelectric and photoelectric properties mentioned in the introductory chapter.

2.1 State of the Art of Biosensors Related to TNF- α Cytokine Detection and Current Devices' Limitations

A current method commonly available for TNF- α concentration detection is applying the Enzyme-linked Immunosorbent Assay (ELISA) kit. ELISA is a widely used laboratory technique for detecting protein molecules [17, 18]. It relies on the specific binding of antibodies to their target proteins [17, 18]. In preparation, a sample containing target antigens is coated on a substrate. The antigen-antibody interactions serve as the primary binding. This binding gets recognized by a secondary antibody, which is linked to an enzyme. The enzyme indirectly binds to the target antigen. Now, while non-bonded enzymes are washed away, adding a substrate solution containing a chromogenic, or color-changing substance will reveal the presence of the enzyme as the enzyme catalyzes the reaction that produces a detectable signal, or a color change [18]. The intensity of the color would be directly proportional to the amount of antigen present in the sample [17, 18].

ELISA's sensitivity depends on the sensitivity of detecting enzymes. Using a well-defined substrate for an enzyme marker will produce accurate ELISA results [17]. For instance, the ELISA MAXTM Deluxe Set Human TNF- α provided by BioLegend states a standard range from 7.8 *pg/mL* (0.45 *pM*) to 500 *pg/mL* (29 *pM*) with a sensitivity of 2 *pg/mL* (0.1 *pM*) [19]. ABCAM's human TNF- α ELISA kit states a detection range from 16 *pg/mL* (0.9 *pM*) to 1000 *pg/mL* (58 *pM*) with a sensitivity of 4.3 *pg/mL* (0.25 *pM*) [21]. Also, the nature of the ELISA technique makes it a heterogeneous immunoassay [17]. The non-reacting substances are washed away before the final signal detection, which improves the selectivity of the sensing technique [17]. Other advantages of ELISA include the scalability and simplicity of the equipment [17]. However, the ELISA kits are generally expensive, with BioLegend selling their MAX Deluxe set at 300 USD and ABCAM selling their kit at 550 USD [19, 21]. The assay time is relatively long, ranging from 1.5 hours to overnight, depending on the specific product [20, 21].

Other methods that have been investigated include variations of immunosensors and electrochemical biosensors, which do not have related products available on the market. These techniques use antibodies or inorganic substances specific to TNF- α to detect the cytokine's presence [22-24]. TNF- α binding to the substance on the sensor surface may generate a measurable signal or initiate changes to the electrical properties at the binding site [22-24]. Capturing the signal generated or characterizing the change in surface properties provides ways of detecting the TNF- α introduced. This later detection method is the approach adopted by the paper.

The immunosensors generally involve functionalization on the solid substrate surface. For instance, Barhoumi et al. reported fabrication based on gold substrates [23]. They electro-addressed anti-TNF- α antibodies onto the gold electrodes and introduced a secondary antibody labeled with horseradish peroxidase [23]. The detection of TNF- α was conducted with a sandwich-type strategy using the two antibodies, and they observed various parameter changes and looked for patterns [23]. In another study, Mazloun-Ardakani et al. developed an immunosensor based on functionalized carbon nanotubes and ionic liquids [24]. An electrocatalyst is introduced for oxidation reaction as a control [24]. The presence of TNF- α antigen binding to the anti-TNF- α on the surface obstructs the electrocatalyst from reaching the reaction site, which changes various parameters, including electrode surface area and electron transfer rate [24].

2.2 State of the Art of NaCl (aq.) Concentration Detection and Corresponding Limitations

The electric response at the interface between an NaCl (aq.) droplet and an n-type silicon surface is investigated before cytokine detection. It would not be surprising to find numerous different methods of detecting NaCl concentrations. However, it would also be likely that the methods suitable for low-concentration detection will suffer from low market demand and high production costs. The products on the market are generally designed to measure the salt concentration in parts per thousand (PPT), which is from tens of millimolar to molar, assuming all the salt dissolved has a molar mass of tens of grams per mole. An example is a salinity refractometer. It measures the change in light refractive index as salt concentration changes [25]. A salinity refractometer is commonly sold for \$40 in North America.

This study proposes an approach for determining solution concentration based on the change in electric properties at the liquid-solid heterojunction. As a variation of the electrochemical biosensing method, this approach leverages the alteration of transient responses for pyroelectric currents and the change in steady-state responses for photoelectric currents. It offers distinct advantages over commercially practiced techniques. The ELISA method employed for TNF- α concentration determination comes with substantial drawbacks. It is both expensive and time-consuming for result analysis. On the other hand, market-available methods for determining NaCl (aq.) concentration face limitations in reaching the low-concentration range, which leaves gaps for emerging solutions. In contrast, this study aims to provide a low-cost and rapid response alternative within the picomolar range of accuracy for TNF- α solutions and in the picomolar to micromolar range for NaCl solutions.

Chapter 3: Materials and Methods

Chapter 3 lists the materials and describes the methods used in constructing the TNF- α /NaCl (aq.) biosensor. It encompasses a thorough explanation of the electronic component design for the biosensor. This chapter also outlines the experimental steps employed for data collection.

3.1 LED as Pyroelectric and Photoelectric Effects' Triggering Source

The triggering source for pyroelectric and photoelectric effects at the liquid-solid interface is an LED light bulb, where both the emitted wavelength and the light intensity are considered for facilitating electric response generation. Pyroelectric response is due to a sudden change in temperature at the site of interest. Hence, obtaining an LED with a higher intensity at a constrained distance is preferred over an LED with a lower intensity. On the other hand, photoelectric response requires photons to hit the interface with sufficient energy to migrate charge carriers from the valance band to the conduction band, which is 1.11 eV for silicon [26]. Potential options for the light source are the following LED bulbs shown in Table 1.

Table 1. LED candidates.

Color	Wavelength (nm)	Photon Energy (eV)	Rated voltage (V)	Intensity (mW/cm ²)
Blue	470	2.64	3.2	18.2
Red	660	1.88	1.8	2.30
Near-infrared	880	1.41	1.5	2.00

The photon energy is calculated using

$$E = \frac{hc}{\lambda},$$

where h is Plank's constant and c is the speed of light. Photons emitted at these three wavelengths carry energy higher than the band gap of silicon at 1.11 eV [26]. The intensities are measured using a Newport power/energy meter with the detector placed approximately 1 cm away from the LED bulbs. The blue LED is preferred because it has the highest rated voltage, which leads to a high intensity at a fixed distance. Hence, it is expected to trigger a more significant pyroelectric transient response relative to the red and the near-infrared LEDs.

3.2 Solution Preparation

The two types of solutions used for analyzing the electric response as a function of the concentration are NaCl (aq.) solution and TNF- α cytokine protein solution. To prepare the NaCl solutions, 0.584 grams of NaCl crystal is dissolved in 10 mL of de-ionized (DI) water to make a 1-molar NaCl solution. Subsequent dilutions shown in Appendix A give NaCl solutions ranging from millimolar to picomolar. The 0-molar NaCl solution would be DI water.

The cytokine protein solutions are prepared similarly. The protein is kept frozen in a fridge to prevent degradation. Each vial contains 20 μL of cytokine at 23 $\mu\text{g}/\text{mL}$. While the molecular mass of TNF- α protein is 17.3 kg/mol , 72 μL of phosphate-buffered saline (PBS) is added to the vial to dilute the solution to 5 $\mu\text{g}/\text{mL}$, corresponding to 300 nM in concentration. Subsequent dilutions with PBS give cytokine protein solutions ranging from nanomolar to femtomolar. Detailed ratios are shown in Appendix B. The 0-molar cytokine solution would be PBS.

3.3 Substrate Preparation

3.3.1 Silicon for NaCl (aq.)

The solid substrate associated with the NaCl solutions starts with a piece of bare n-type silicon with a thin layer of native oxide at approximately 1 to 2 nm [27]. The liquid-solid interface area is initially defined by masking the silicon surface with a layer of thick oxide and opening 3 mm by 3 mm square windows, as shown in Figure 1. Figure 1 left shows a 3D drawing, and right shows a substrate sample used for measurement. This way, although the liquid droplet may spread uncontrollably, if the square window is fully covered, the interface area is well-defined. One end of the substrate is sputtered with aluminum for solid probe contact. Streaks of aluminum run across the square windows and end at the left end of the substrate to ensure connectivity.

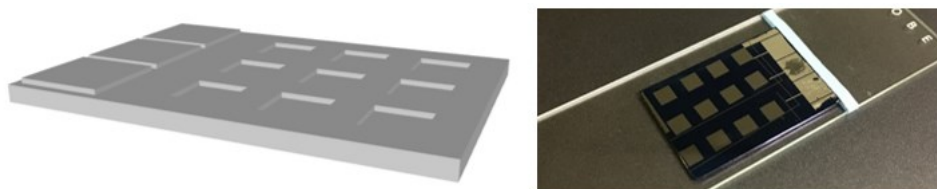


Figure 1. Silicon substrate with surface features for interface area definition and solid probe contact: 3D drawing (left) and sample substrate (right).

However, such a method of defining contact degrades over time as the solid contact probe scratches on the sputtered aluminum. The connection becomes unreliable as the layer of aluminum wears off. Hence, the simple solution is to stay with the bare n-type silicon and define the interface area with a PDMS well, which will be introduced in Section 3.5. One spot close to the edge is designated for probing. This spot is scratched with a diamond pen to remove native oxide that would block the solid contact.

3.3.2 Aptamer Functionalization on Silicon with an Oxide Layer for Cytokine Solution

Functionalizing the substrate's surface with aptamers to pick up cytokine molecules starts with a piece of n-type silicon coated with a thin layer of aluminum oxide (Al_2O_3). The Al_2O_3 -coated silicon is treated with an aminopropyl triethoxysilane (APTES) solution, a glutaraldehyde (GA) solution, and a fluorescent aptamer solution, respectively. Resting the substrate in the APTES and GA solutions plants organic linkers on the substrate's surface and leaving it in the fluorescent aptamer solution overnight completes the functionalization.

Please refer to Appendix C for detailed instructions on the procedure.

Figure 2 shows a functionalized substrate shined by a blue laser. The fluorescent aptamer planted onto the silicon substrate surface absorbs blue light and emits green light. Figure 2 left is captured without a color filter. The blue spot would look the same regardless of the functionalization process as the silicon surface reflects the light. Figure 2 right is captured with a color filter absorbing light in the visible range from purple to 532-nm green. The green dot's presence is due to aptamer's light emission, whereas if the sample is a piece of bare silicon, the green dot would not appear.

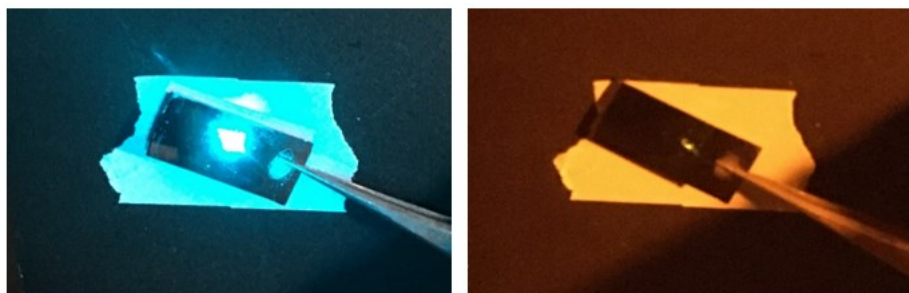


Figure 2. Functionalized silicon substrate shined by a blue laser: picture taken without the filter (left) and with the filter (right).

3.4 Constraining the Liquid-solid Interface Area with PDMS

A polydimethylsiloxane (PDMS) device is attached to the surface of an n-type silicon substrate to constrain the liquid-solid interface area. The PDMS device is shaped into a square well, where a solution droplet contacts the substrate at the bottom of the well only. The interface area is defined by the horizontal cross-section of the well. Also, surrounding the solution with PDMS reduces liquid evaporation during a measurement since it reduces the droplet's surface air exposure.

Figure 3 shows the 3D drawings for the mold used to shape the PDMS, and Figure 4 shows the PDMS well. The square-well pattern was originally designed to match the etched window on the silicon substrate with an oxide mask. It provides the same constraint on the interface for unmasked silicon. The wells are 3 mm by 3 mm for cross-sectional size and 3 mm deep. Each well shall contain up to 27 μL of solution. Appendix D shows detailed information on curing PDMS and baking the PDMS device. Appendix G presents the projection views of the 3D-printed parts with dimensions.



Figure 3. Drawings of PDMS device mold: side piece (left) and bottom piece (right).

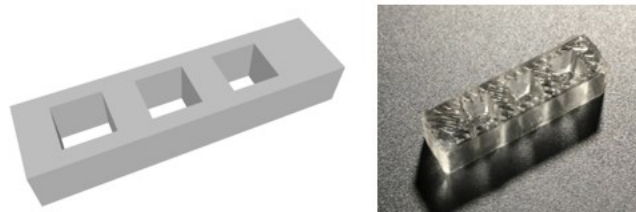


Figure 4. PDMS square well: 3D drawings (left) and baked device (right).

While the mixed PDMS is poured into the mold, a small gap between the side and the bottom pieces will cause a certain amount of leakage when the PDMS is baked in an oven. Hence, the top of the PDMS device may not be even, and the well will contain less liquid than designed. Figure 5 shows a finished well with an uneven top mounted on a silicon substrate with tape holding it against the substrate. It contains about 24 μL of solution. The tape should press the PDMS tightly against the substrate surface so that there will not be any leakage seeping through the bottom of the well.



Figure 5. PDMS square well mounted on a silicon substrate using tape.

3.5 Experiment Setup

Measuring the pyroelectric and photoelectric currents generated at the interface involves a circuit setup shown in Figure 6. The arrangement applies to both NaCl (aq.) on silicon and cytokine solutions on functionalized silicon. Although the drawing shows a solution droplet placed directly on the substrate, it is placed in the PDMS device during the experiment. The probe connecting the liquid end has its tip suspended in the solution droplet. The probe connecting the solid end taps either on the aluminum contact if an aluminum-sputtered area is available, or directly on the substrate. The two probes pick up the electric current generated at the liquid-solid interface. An LED bulb is placed above the droplet to trigger the current generation. Section 3.6 elaborates on the various methods used in reading the current signal.

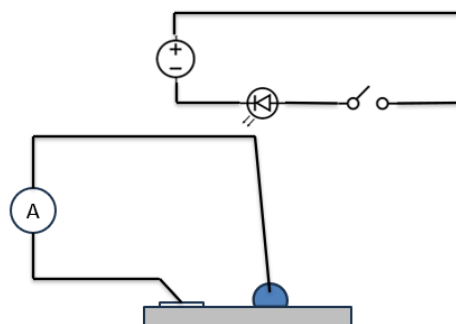


Figure 6. Schematic diagram for pyroelectric and photoelectric current generation.

Figure 7 shows a probe arrangement for the pyroelectric and photoelectric current measurement. Here, a tungsten or copper probe serves as the liquid probe, and a spring-loaded gold-coated tip serves as the solid probe.

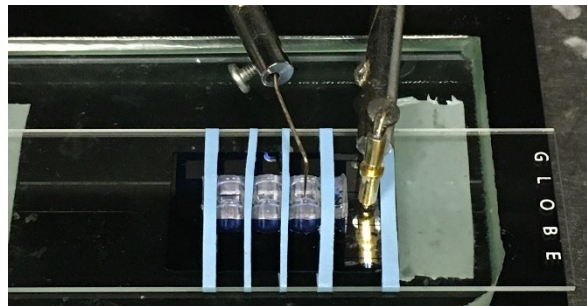


Figure 7. Pyroelectric and photoelectric current measurement setup: positioning the contact probes.

3.6 Methods of Electrical Signal Measurement

The current generated at the interface due to changes in temperature and light exposure is small, and there needs to be an effective method of reading the current signal. Options for the signal measurement tool include a source meter, an oscilloscope, and a customized high-rate analog-to-digital converter (ADC). The schematic block diagrams for the circuit connection associated with each measuring method are shown in Figure 8.

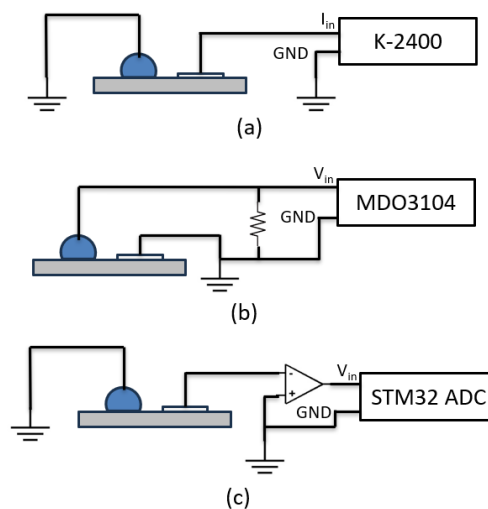


Figure 8. Schematic block diagrams of circuits used for three signal measuring methods: (a) using a source meter. (b) using an oscilloscope, and (c) using an ADC.

Figure 8 (a) uses a Keithley 2400 Source Meter to acquire the current signals directly with nanoamps precision. Users can feed the current to the input end of the source meter and use the desktop application Keithley KickStart to obtain a current vs. time curve. No extra element for the circuit is required, and the current obtained is the current generated at the interface.

The second option is to use an oscilloscope to capture the waveform of the current signal over time, as shown in Figure 8 (b). The Tektronix MDO3104 oscilloscope comes with a high sampling rate, which provides convenience in obtaining the transient peak. However, the

oscilloscope only measures the voltage signal, and the finest voltage amplitude is in the millivolts range. In this case, a large resistor with resistance in the megaohms range needs to be added between the liquid and the solid electrodes. The oscilloscope probes are connected in parallel with the resistor. They pick up the voltage signal driven across the resistor by the current coming from the liquid-solid interface.

To package the liquid-solid device and the signal measuring tool as a portable entity, the probes can be connected to a customized high-rate ADC for data acquisition. In Figure 8 (c), the generated current is first fed to a pre-amplifier to amplify the signal level from nanoamps to volts. The signal then goes through a low-pass filter with a cutoff frequency of several hundred hertz to eliminate sharp noise. An ADC port on a microcontroller development board accepts the signal. The ADC samples and quantizes the input at a customized rate, and the microcontroller further processes the buffered data. The following section describes the details on building this sensor prototype entity.

3.7 Biosensor Prototype Design and Assembly

The portable entity combining the liquid-solid device and the signal measuring tool mentioned at the end of the previous section is the biosensor prototype box that this project aims to build. While collecting data, the biosensor box outputs the transient peak value of the electric response due to the pyroelectric or triboelectric effect at the liquid-solid interface for solutions with known concentrations. These data are filled into a look-up table relating the transient peak value and the solution concentration. Later, when data collection is complete, inputting a solution with an unknown concentration within the defined range to the biosensor box will have its transient value matched to an interpolated value from the look-up table. Hence, the biosensor box can output the estimated substance concentration for the unknown solution.

3.7.1 Circuit Design

The schematic diagram drawn in Figure 9 shows the circuit design of the biosensor box. The liquid-solid device (U3) generates a small electric current that gets amplified through the transimpedance amplifier (TIA) (U1A). The current signal in nanoamps becomes a voltage signal in millivolts at the output of the TIA. The active low-pass filter (LPF) (U1B) has a cutoff frequency of 400 Hz, which cleans some of the sharp noise through the transient response while keeping the transient peak. The voltage signal then feeds the ADC port on an STM32 microcontroller (U2B1), where programming takes care of the rest.

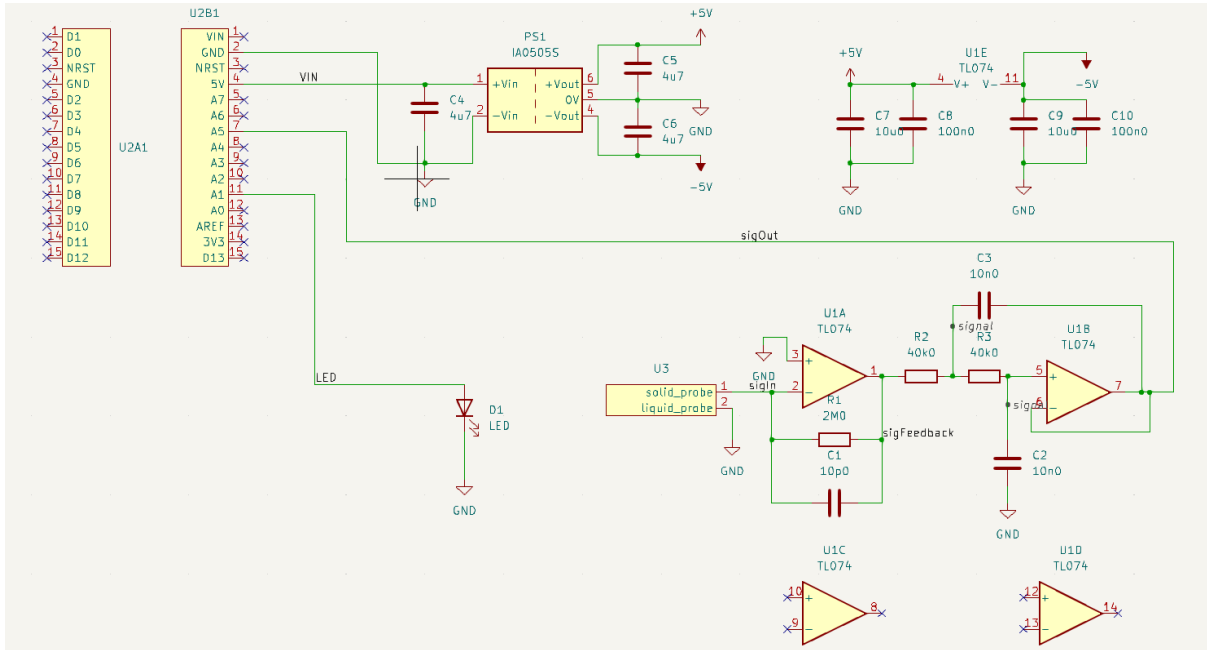


Figure 9. Biosensor box circuit schematic diagram.

The DC-DC converter (PS1) takes +5V from the STM32 board and supplies +5V and -5V to the amplifiers. The GPIO port A1 on the STM32 gives a square wave at a customized frequency and 3.2V peak-to-peak voltage to blink the LED (D1).

Among the selected components, the TL074 general-purpose operational amplifier is picked for its gain-bandwidth product (GBW) and power consumption. It offers a GBW at 3 MHz typical, which ensures the transient response remains well-preserved after amplification [28]. It operates at a relatively low power consumption rate, drawing 1.4 to 2.5 mA of current per amplifier [28]. With two amplifiers in use, the power consumption rate is expected to be in tens of milliwatts. For the microcontroller unit, the STM32 L432 Nucleo board is selected mainly because its built-in ADC module offers a high sampling rate of up to a million samples per second at a 12-bit resolution [29]. This ensures consistency in capturing the transient response's peak value. Moreover, the STM32 Nucleo board supports UART serial communication, facilitating output display on a computer console [29]. In addressing the DC-DC conversion requirement, the IA0505S converter suffices the need by outputting a relatively stable +5 V and -5 V from a +5 V input [30]. These components are also cost-effective, with the TL074HIDR 14SOIC listed at 0.609 CAD, the STM32 NUCLEO-L432KC at 16.43 CAD, and the IA0505S-1WR3 at 6.93 CAD [31].

Figure 10 shows the circuit implemented on a breadboard and the parts connected off the board. The liquid contact probe, the solid contact probe, and the LED setup are the same as when the measuring tool is a source meter or an oscilloscope. The STM32 microcontroller connects to a laptop via USB-micro for power and data transmission. The breadboard connection in this figure skips the LPF, that the TIA outputs straight to the STM32 ADC port for testing purposes.

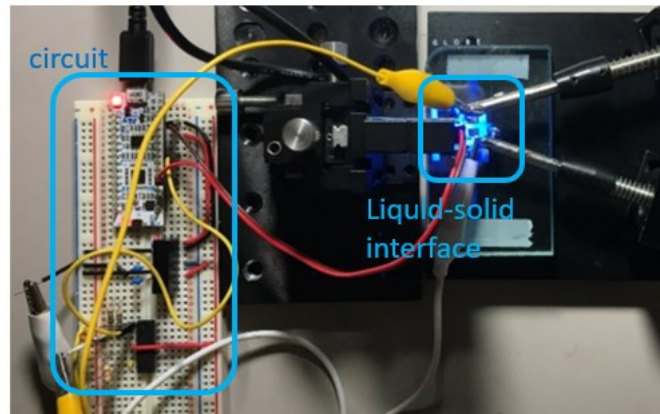


Figure 10. Breadboard implementation of the biosensor box circuit with probes.

The circuit is transferred to a printed circuit board (PCB) to reduce parasitic capacitance and inductance, improve heat dissipation, and reduce the size such that all components can be packed into a box. Figure 11 shows the PCB design's front and back. The liquid and solid probes are connected to the pin sockets at U3. U3's positive end feeds the signal to the TIA and the LPF built using a TL074 chip. After the pre-amplifier, the signal goes to the microcontroller's socket ADC1 (back side top row, 7th pin counting from the right). The black box on the front's top left corner is the DC-DC converter.

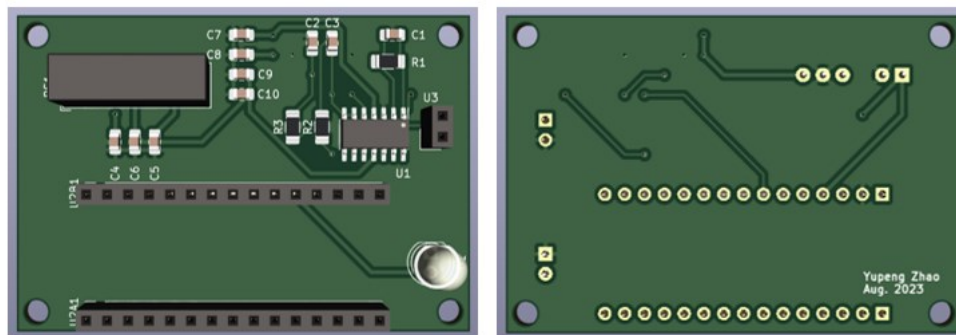


Figure 11. PCB design, front (left) and back (right).

3.7.2 Programming Design

An STM32 Nucleo development board is most conveniently programmed with C/C++. It uses the STM32CubeIDE as the development platform, including peripheral configuration, code generation, code compilation, and debug features. The peripherals associated with the biosensor box are the liquid-solid interface and the LED, connected to an ADC port and a general-purpose input-output (GPIO) pin on the STM32 board, respectively. Also, the biosensor box communicates with a laptop computer via UART serial to print the console outputs.

Figure 12 shows a flowchart summarizing the software design. After the initialization, the program starts the timer, which triggers the ADC reading and the direct memory access (DMA) writing cycle. The program utilizes the circular buffer technique to record the input

data. The circular buffer is divided into two halves, where it uses callback functions to check the fill-in status. The callback functions will execute data manipulation for the half-filled buffer, and when the buffer is full, it will also call for a new ADC reading cycle, overwriting the buffer with new inputs.

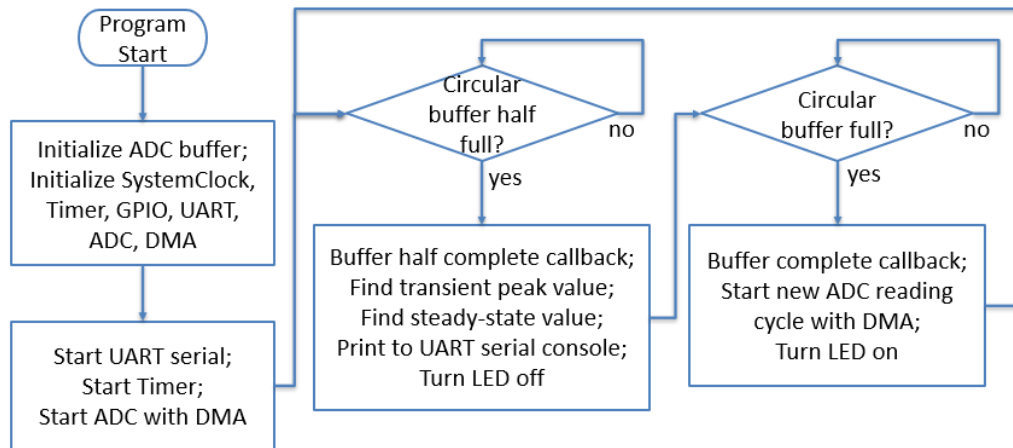


Figure 12. Program flowchart for customized ADC and data post-processing.

Notice that the ADC reading and the DMA writing do not pulse when the callback functions execute data manipulation commands. Incoming ADC conversions are recorded in the second half of the circular buffer, while the electric response values are extracted from the first half. STMicroelectronics states their STM32L4 ADC block can achieve a maximum of 5.33 mega-samples per second at a 12-bit resolution [32]. Such a rate is not necessary, whereas one kilo-sample per second suffices the biosensor's need of capturing the transient peak value.

For this program, the ADC clock is connected to the timer clock by setting the ADC conversion as a time-triggering event. The timer clock is driving at 32 MHz. The pre-scaler (PSC) is assigned 9. The counter period, or auto-reload register (ARR), is assigned 1999. Then the sampling frequency is computed as

$$f_{sampling} = \frac{timerCLK}{(PSC + 1) \cdot (ARR + 1)} = \frac{32 \text{ MHz}}{(9 + 1) \cdot (1999 + 1)} = 1600 \text{ Hz.}$$

While the allocation length for the circular buffer is 10000, completing one reading cycle takes about 6 seconds, or 3 seconds to fill half of the buffer. Hence, there are another 3 seconds for the callback function to find the transient peak and/or the steady-state values when filling the first half is done, which is more than enough time to complete the task.

While the ADC pipeline is well-defined with the microcontroller's timer and the buffer callback functions, defining the LED pulse is straightforward. The LED is connected to GPIO pin A1. The cycle begins with the microcontroller not knowing the state of the LED. As the ADC buffer is halfway filled up, the half-transfer callback function wakes, and the microcontroller sends a RESET to GPIO A1, turning the LED off. The ADC keeps filling the

circular buffer. When the buffer is full, the full-conversion callback function wakes, initiating another ADC conversion via DMA, and the microcontroller sends a SET to GPIO A1, turning the LED on. This way, the LED turns off and on exactly once throughout an ADC reading cycle, synchronizing the response reading with the effect trigger.

3.7.3 Casing Design

The biosensor prototype casing is designed using 3D printing technology to achieve quick delivery with precision in dimensions. The design prioritizes functionality, where parts are composed of simple geometric shapes and ensures easy assembly. The main emphasis of the design is on the secure placement of the liquid-solid device, the contact probes, and the LED bulb within the biosensor box. The finished box is 100 mm by 60 mm by 100 mm. Figure 13 lists all the 3D-printed parts used in the box assembly, and Appendix G provides details in dimensions.

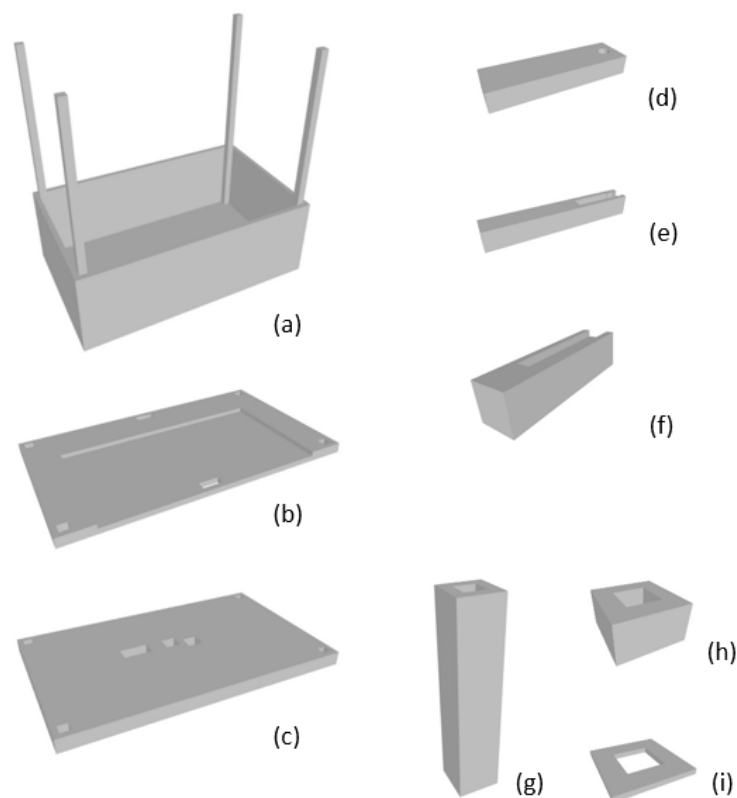


Figure 13. Biosensor casing parts: (a) Base piece, (b) substrate holder, (c) lid, (d) liquid probe support, (e) solid probe support, (f) LED holder, (g) square stand 32-0, (h) square stand 4-0, and (i) square washer 0-5.

Figure 14 shows an assembled biosensor box. The base design does not have any holes reserved for screws or a USB mini plug-in slot. These holes shall be drilled according to the exact location where the PCB board rests. Drilling may also be required for the substrate holder, depending on the wire positions that extend out of the box. If the poles sticking out of the base are rough due to 3D-printing's nature, sand them with fine sandpaper such that the substrate holder and the lid can be mounted on the base. The spring-loaded probe for solid

contact resists the lid from closing onto the square washers. Place a weight on the lid to press the spring-loaded probe down against the substrate.

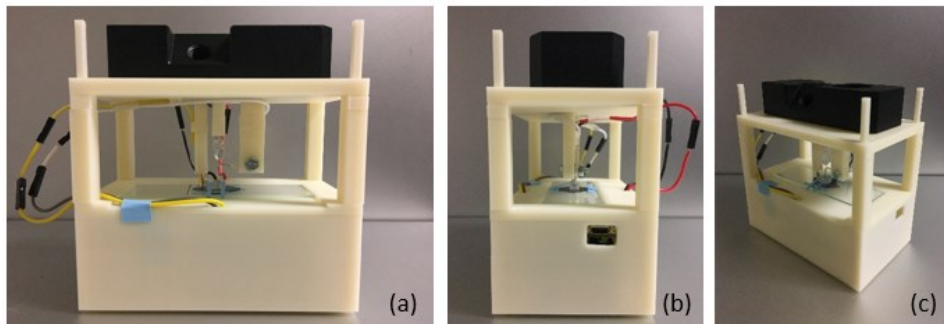


Figure 14. Assembled biosensor box: (a) front, (b) right, and (c) isometric.

3.8 Notes on Cleaning Procedures

The experiment setup varies depending on the specific type of measuring tool involved. However, the procedure used to establish the liquid-solid interface is the same regardless of the rest of the circuit. Showing some creativity may also help when certain components are introducing extra constraints during the setup. Apart from positioning the solid substrate, the solution droplet, the LED, the probes, and the circuit, there are a few more remarks on cleaning the substrate during and after an experiment.

3.8.1 Cleaning During an Experiment

The experiment measures the electric properties at the interface for a series of solution concentrations. Placing and removing the droplet in the order of ascending concentration reduces cross-contamination. Hence, the same solid substrate can be used throughout without replacement. However, cleaning is still required to eliminate solution residue left from the previous concentration. This can be achieved with the following steps.

1. Draw the solution out of the PDMS well with a micropipette. Reach to the corners and remove as much residue as possible.
2. Fill the PDMS well with DI water (for NaCl) or MBG water (for cytokine) using a syringe.
3. Draw and place the liquid repetitively with a micropipette. Repeat steps 2 to 3 a few times.
4. Blow dry the PDMS well with inert gas. If compressed gas is unavailable, blow dry with air using an empty squeeze bottle or a pipette bulb.

These steps only wash the inside of the PDMS well to avoid removing the tapes securing the PDMS device against the solid substrate.

3.8.2 Cleaning After an Experiment

Performing a substrate clean after a cycle of interface measurement aims to remove any residual substances such that substrates provide accurate data for the next measuring cycle. For n-type silicon with NaCl solution droplets placed, the cleaning procedure is simply an

acetone wash, an isopropyl alcohol (IPA) wash, and a DI water wash, followed by blow drying with an inert gas. Sodium and chloride ions dissolved in water are highly mobile and get rinsed off the surface after these washes, along with any potential organic contaminants. For functionalized silicon with cytokine solutions, substrates are single-use because cleaning them would involve breaking the bonds between cytokines and aptamers while keeping the bonds between oxides and organic linkers, as well as between organic linkers and aptamers. The easiest way to prepare substrates for the next measuring cycle is to functionalize new substrates with aptamers.

Chapter 4: Results

Chapter 4 presents the outcomes of the experimental investigations. The collected data are organized to illustrate the electric responses as functions of NaCl solution concentration and TNF- α solution concentration. Readings from the source meter, the oscilloscope, and the biosensor are visualized using appropriate figures.

4.1 Pyroelectric and Photoelectric Responses observed using a Source Meter

The two electrodes of the liquid-solid interface are directly connected to the input of a Keithley source meter. Ground the liquid contact and take signals from the solid contact such that the response shows positive values for the duration of the LED being ON. On the driver application, choose 0 bias voltage and plot the current over time. Figure 15 shows an example of the current signal collected from a source meter. Here, a red 660 nm LED is manually controlled with a DC power supply, sustaining ON for approximately 8 seconds and OFF for 8 seconds. Over the 90 seconds, the source meter samples 1000 points, capturing 5.5 periods. The main issue with this setup is revealed in this data set. The source meter's sampling rate of 11 samples per second is too low to capture the transient response reliably. It only shows consistency for the steady-state value, corresponding to the photoelectric current. Another piece of information Figure 15 provides is that the photoelectric steady-state current responses are in the range of tens of nanoamps, and transient peak values may be in large tens to hundreds of nanoamps. Hence, subsequent setups have abandoned the source meter and turned to other devices for data collection.

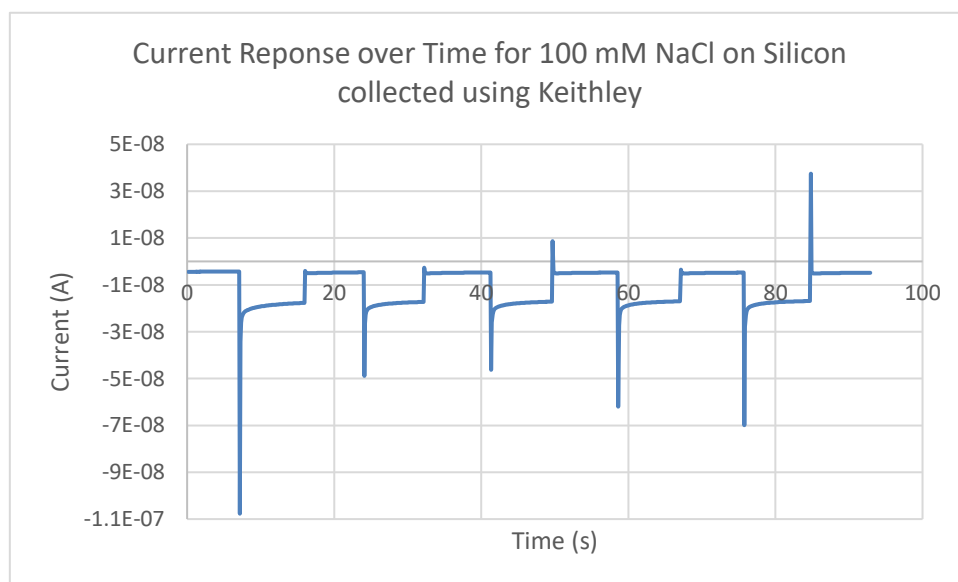


Figure 15. Current readings collected from a Keithley source meter subjected to 100 mM NaCl (aq.) on silicon.

4.2 NaCl (aq.) on Silicon, Pyroelectric and Photoelectric Responses observed using an Oscilloscope

An oscilloscope displays the voltage difference across its input and the ground. To effectively measure the electric current signal generated at the liquid-solid interface, the current is passed through a 15-M Ω resistor, and the oscilloscope measures the resulting voltage signal. Figure 16 shows the voltage readings collected under a 470 nm blue LED for an assorted list of NaCl (aq.) concentrations. A function generator outputting a square wave at 150 mHz and 3.2 peak-to-peak voltage toggles the LED bulb every 3 seconds. The oscilloscope samples at 500 samples per second and acquires 10k data per window. Each window captures approximately 6 periods. In contrast to the source meter, the transient peaks' heights are consistent for each solution concentration. Data collected at a rate of 500 samples per second or higher can be used for comparison across concentrations.

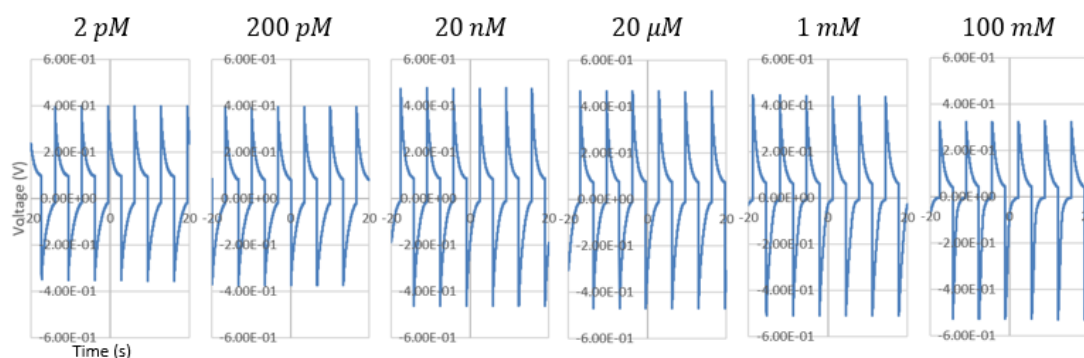


Figure 16. Voltage readings collected from a Tektronix oscilloscope with NaCl solution concentrations at 2 pM, 200 pM, 20 nM, 20 μ M, 1 mM, and 100 mM.

To obtain positive signal responses for the duration of the LED is ON, the liquid contact needs to feed the signal to the oscilloscope's input, whereas the solid contact is grounded. The configuration is opposite to that of the source meter. Knowing an oscilloscope displays a given waveform upright, the source meter may have at least one inverting pre-amplifier at its input.

Notice although a voltage measuring device shall have an infinite input impedance in the ideal case, its finite impedance takes account of splitting the current passing through the device under test. The Tektronix MDO3000 Series oscilloscope equipped with the TPP Series passive voltage probes has nominal input impedance of 10 M Ω [33]. Hence, converting a voltage reading displayed on the oscilloscope to the current generated at the liquid-solid interface requires the following calculation:

$$I_{interface} = V_o \cdot \left(\frac{1}{R_{osc}} + \frac{1}{R_L} \right) = V_o \cdot \left(\frac{R_L + R_{osc}}{R_L \cdot R_{osc}} \right),$$

where V_o is the displayed voltage, R_L is the 15-M Ω load resistor, and R_{osc} is the 10-M Ω input impedance.

Figure 17¹ shows the change in the current response level over NaCl solution concentration for three different LED wavelengths and two different intensities. The horizontal axis is plotted over a log scale. The intensity is controlled using a Thorlabs variable neutral-density filter. The transient peak value is the sum of the pyroelectric and the photoelectric current. The steady-state value is the photoelectric current only. In both plots, the 470 nm LED with the greater intensity gives the highest response level. The 470 nm curve is used for calculating the sensitivity in the following analysis.

Figure 17 (a) shows that the transient peak value stays flat and increases in the picomolar to nanomolar range. It stays flat again over the micromolar range and drops in the millimolar range. The sensitivities of these sections are calculated by simply finding the slope of the best-fit line. From 200 *pM* to 20 *nM*, the sensitivity is 4.8 *nA* per decade. From 100 *μM* to 100 *mM*, the sensitivity is -8.0 *nA* per decade, negative due to a decreasing transient peak. This does not characterize a good sensor, as the change in response is not monotonic over the shown concentration range. The sensor cannot associate a transient value with at most one concentration. Moreover, there is a 4-decade range in the micromolar region where the transient value stays constant. Targeting the low-concentration end, this sensor would be useful if a given solution sample is known to have a NaCl (aq.) concentration of less than 20 *nM*.

Figure 17 (b) shows the steady-state photoelectric current values having an overall decrease as NaCl solution concentration increases. Based on the 470 nm blue LED with the greater intensity, the sensitivity is -0.64 *nA* per decade over the range from 2 *pM* to 100 *mM*. However, the slope is relatively shallow for the section before 100 *μM* (-0.38 *nA* per decade) and steep after 100 *μM* (-1.9 *nA* per decade). With about two-thirds of the overall decrease occurring in the millimolar range, the sensor is unreliable near the low-concentration end². However, if it is used together with the pattern observed from the transient peak values, the observed decrease in the steady-state response may help construct an NaCl (aq.) concentration sensor. Chapter 5 will further discuss the details.

¹ Figure 19 does not show the point for 0 M NaCl (aq.), DI water, because the log scale does not plot a zero. Audiences may refer to Appendix H for the data.

² Audiences may have noticed an increase of 5 folds in solution concentration from 20 *μM* to 100 *μM*, whereas increases are of 10 folds everywhere else. This is due to a change in scale at the early experiment stage. Initially, I measured electric responses with respect to changes in concentration over a linear scale, and solutions were diluted to give 20 *μM*, 40 *μM*, 60 *μM*, and 80 *μM*. Later, I decided to vary the concentration over a logarithmic scale. Instead of making a 10 *μM* NaCl solution, I used the 20 *μM* as the source for further dilutions. This was corrected when I switched the measuring tool from the oscilloscope to the biosensor box with a customized ADC.

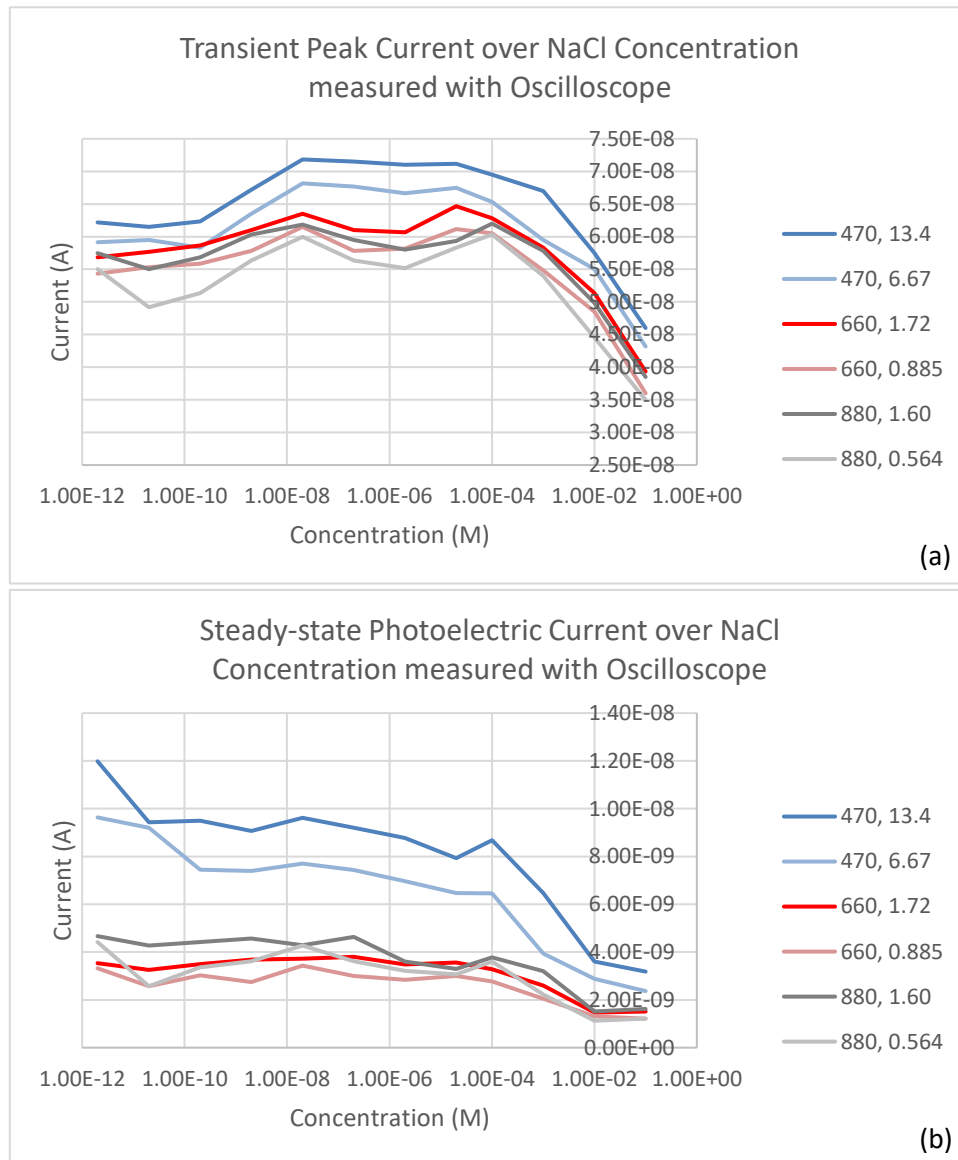


Figure 17. The oscilloscope readings of the current generated at the NaCl (aq.)-silicon interface due to pyroelectric and photoelectric effects: (a) transient response peak values, and (b) steady-state values. The legend on the side indicates the LED wavelength in nm followed by the intensity in mW/cm^2 (e.g. 470, 13.4 is the 470 nm blue LED at 13.4 mW/cm^2).

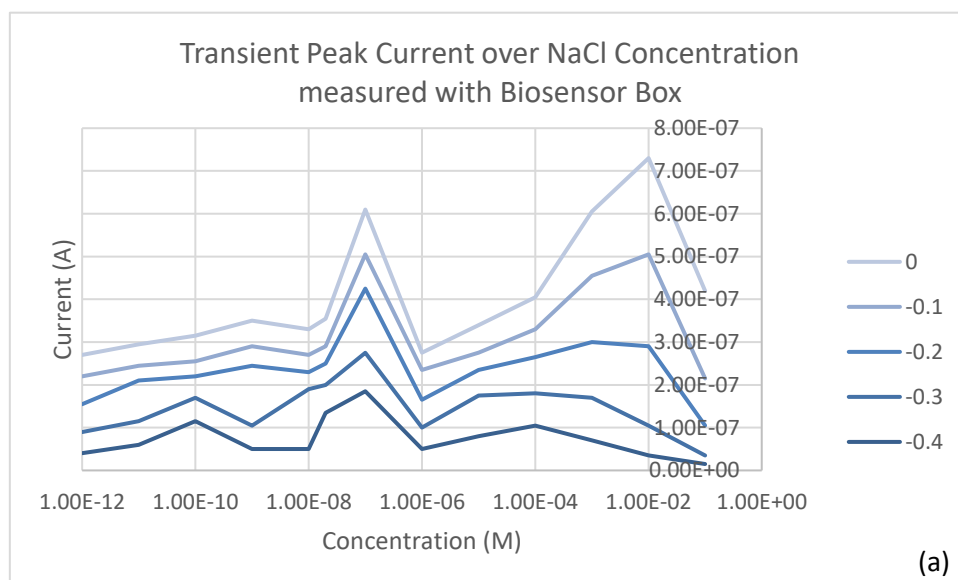
4.3 NaCl (aq.) on Silicon, Pyroelectric and Photoelectric Responses Observed using the Biosensor Box

The customized high-rate analog-to-digital converter (ADC) from the biosensor box is used in place of the oscilloscope to measure the current response at the liquid-solid interface. Since the transimpedance amplifier (TIA) before the ADC input port is inverting, the probe connection needs to be opposite to that of the oscilloscope. The solid contact feeds the current signal to the TIA's inverting input, and the liquid contact is grounded. The TIA's gain is $2 M\Omega$ and outputs a voltage signal in millivolts to volts. The 12-bit ADC reads voltage signals from 0 to 3.3 V with a 1-mV resolution and samples at 1600 samples per second. Figure 18 shows the transient response peak value over NaCl (aq.) concentrations. The data collected with the

biosensor box exhibits a different pattern compared to that of the oscilloscope. Moreover, the transient response decays rapidly, and there is no steady-state response when the LED is sustained to be ON. This is observed by feeding the TIA's voltage output to an oscilloscope. Chapter 5 will further discuss the potential reasons behind the different patterns.

Apart from measuring the signal at the interface as a self-powered device, this data set attempts to seek patterns under biased conditions. The voltage bias is inserted in series with the liquid-solid interface. Since the TIA is inverting the signal, connecting the V_{bias} 's positive end to the ground, negative end to the liquid contact, and providing a positive DC bias elevate the current response. Providing a negative DC reverses the bias condition and suppresses the current response. Figure 18 (a) shows the transient peak values with the V_{bias} set at 0, -0.1, -0.2, -0.3, and -0.4 V. With no biasing voltage applied, the response value has an overall increasing trend at 26.5 nA per decade with increasing solution concentration. The graph has two local peaks. One peak occurs at 100 nM , and the second peak occurs in the millimolar range. This introduces a difficulty for associating one transient value to one concentration. Applying a reverse voltage bias reduces the device's sensitivity while the overall shape of the graph is sustained until -0.3 V of biasing. Table 2 lists the sensitivity for each biasing value.

Figure 18 (b) shows the transient peak values with the V_{bias} set at 0, 0.1, 0.2, 0.3, and 0.4 V. There is a slight difference in the 0 bias graph shown in (b) relative to (a) in terms of the peak's location in the millimolar range. Forward voltage bias increases the device's sensitivity for concentrations higher than $1 \mu\text{M}$. Table 3 lists these sensitivities. The local peak in millimolar vanishes after 0.2 V of biasing. The graph behavior remains the same for concentrations smaller than $1 \mu\text{M}$, and the peak at 100 nM persists.



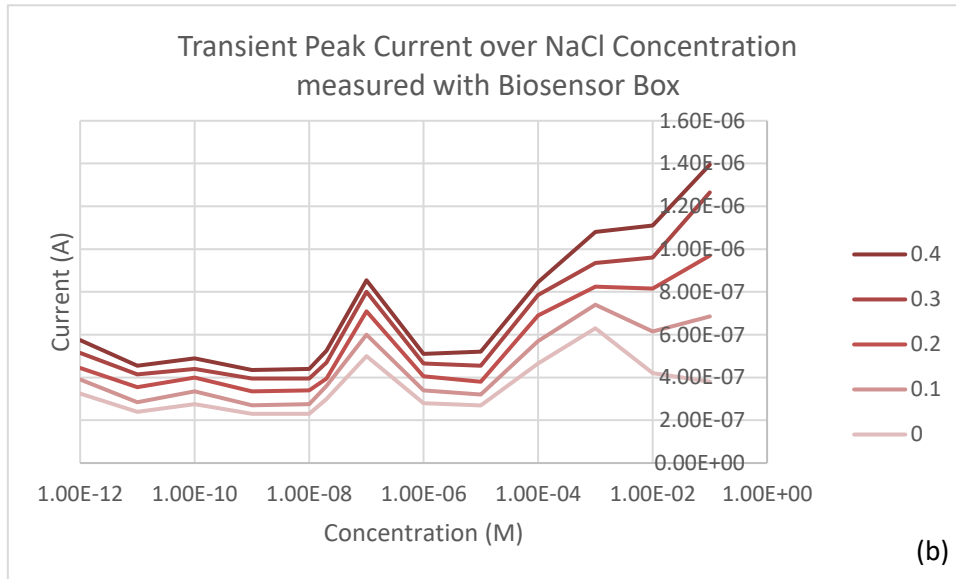


Figure 18. Transient response peak values at the NaCl (aq.)-silicon interface measured using the biosensor box with voltage biases applied in series, including (a) reverse biases up to -0.4 V, and (b) forward biases up to 0.4 V. The legend on the side labels the biasing values.

Table 2. Reverse bias voltages and their corresponding device sensitivity from 1 μM to 100 mM .

Bias (V)	0	-0.1	-0.2	-0.3	-0.4
Selectivity (nA per decade)	26.5	12.7	2.05	-1.89	-2.05

Table 3. Forward bias voltages and their corresponding device sensitivity from 1 μM to 100 mM .

Bias (V)	0	0.1	0.2	0.3	0.4
Selectivity (nA per decade)	31.9	79.4	122	163	184

Connecting the voltage bias in parallel with the liquid-solid interface was also attempted, but the STM microcontroller did not show any readable result through the UART serial console. The serial outputs were distorted with garbled characters.

4.4 Capacitance Measurement at the NaCl (aq.)-silicon Interface

The capacitance at the liquid-solid interface is also investigated for the NaCl solutions. The liquid and solid contacts are connected to a digital multimeter (DMM) to measure the capacitance. Here, the DMM used is the Rigol DM3000 Series, and Figure 19 shows the capacitance over the solution concentration. Instead of plotting the capacitance values, Figure 19 plots the ratios against the capacitance measured for 0-molar (DI water) solution on a silicon substrate. Plotting the ratio neglects the interface's geometry, which is held at a constant for all NaCl (aq.) concentrations. Figure 19 also shows the transient current ratio taken from Figure 18 (a) 0-bias for pattern comparison. Having the same local peaks at 100

nM and in the millimolar suggests that the response peak value picked up by the biosensor box is related to the interface capacitance.

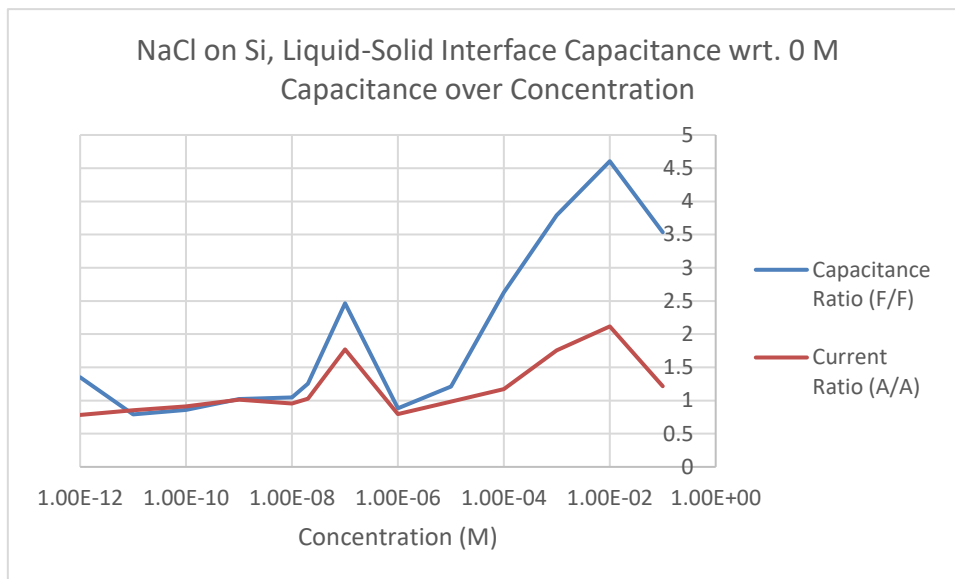


Figure 19. Capacitance measurement at the liquid-solid interface plotted as the ratio against the 0-molar interface capacitance in blue. The transient current peak values collected at 0 bias are also plotted as ratios in red for pattern comparison.

4.5 TNF- α Cytokine on Aptamer-functionalized Silicon, Pyroelectric and Photoelectric Responses Observed using an Oscilloscope

Figure 20 shows a set of current response data from shining a blue LED onto the liquid-solid interface between TNF- α cytokine solutions and an aptamer-functionalized silicon substrate collected using the Tektronix oscilloscope. Neither one of the curves suggests a clear pattern with increasing concentration. The transient peak values shown in (a) have a mean of 49.8 nA and a standard deviation of 1.2 nA . The fluctuation is slight and irregular. The steady-state values shown in (b) have a mean of 15.4 nA and a standard deviation of 4.0 nA . This curve exhibits a rise from the femtomolar to the picomolar range but drops as the cytokine concentration further increases.

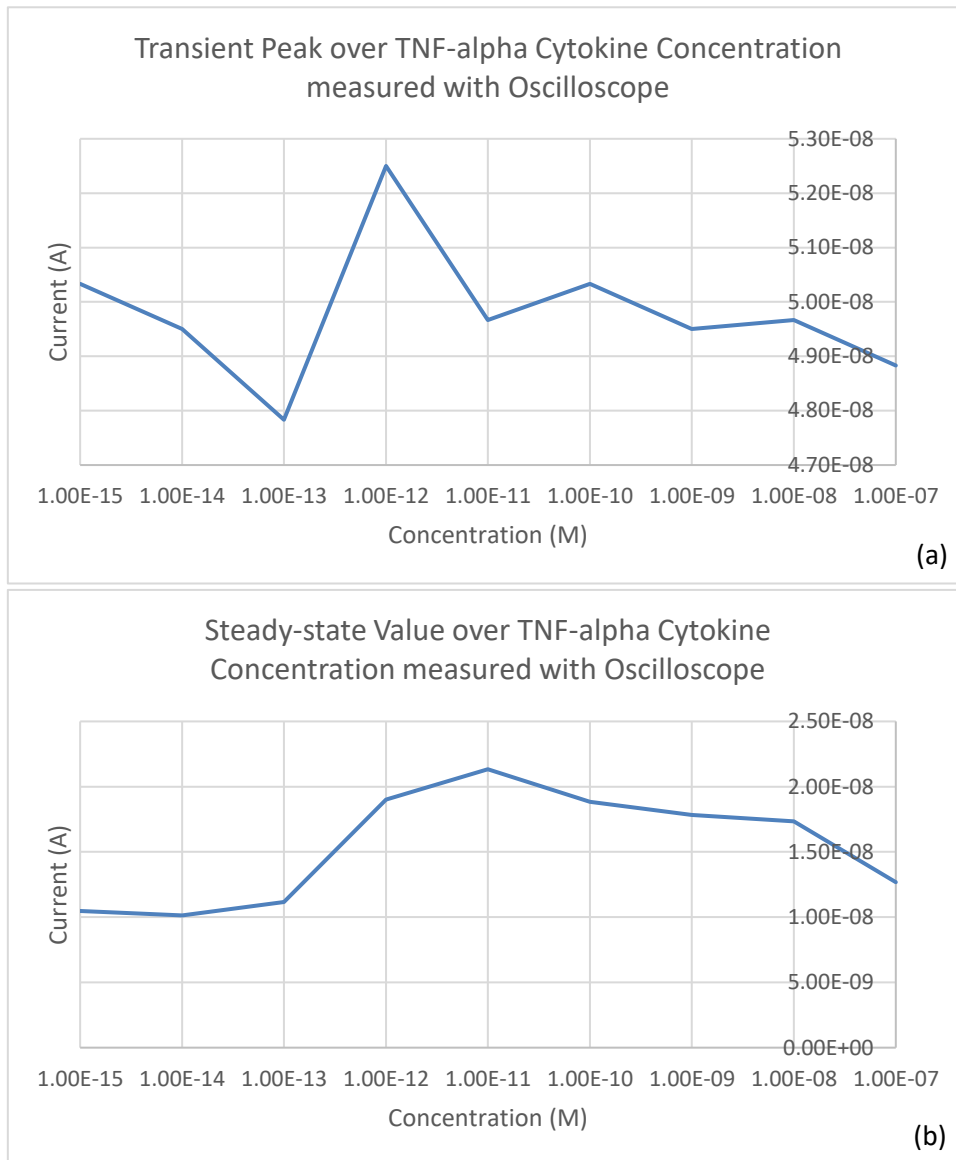


Figure 20. Current response values over cytokine solution concentration at the liquid-solid interface between TNF- α cytokine solution and aptamer-functionalized silicon substrate, showing both (a) transient peaks and (b) steady-state values.

The electric current response collection for TNF- α cytokine solution on functionalized silicon has not been repeated due to time constraints. Confirmation of the curve's shape is necessary with more trials. Together with measuring the cytokine-aptamer interface's current response using the biosensor box, they are recapped in Chapter 5 and saved for future works.

Chapter 5: Discussion, Conclusion, and Future Work

Chapter 5 discusses the results obtained throughout the experiments. It interprets the findings in the context of the research questions and explores the implications of these results. This chapter also addresses limitations encountered during the research and purposes recommendations for future studies based on the outcomes.

5.1 NaCl (aq.) Concentration Sensing

The NaCl (aq.)-silicon interface's pyroelectric and photoelectric current responses collected with the oscilloscope demonstrate usefulness in determining the NaCl (aq.) concentration. Despite Figure 17 showing small changes in both the transient peak and the steady-state value for the micromolar range, combining the transient curve with the steady-state curve can distinguish the picomolar to nanomolar from the millimolar range. For instance, an unknown solution sample generating a 65-nA peak may have a concentration close to either 1 nM or 1 mM, according to Figure 17 (a). Now, looking at Figure 17 (b), if it generates a 9-nA steady-state current, then it is 1 nM, whereas if it generates a lower steady-state current at 6 nA, it would be 1 mM. This provides an option to extend the NaCl (aq.) concentration detection range toward the lower end relative to the market-available refractive method.

Figure 17 (a) shows a positive slope at the lower concentration end, flat at the middle, and a negative slope at the higher end. A hypothetical cause of the change in the trend lies in the number of charge carriers in the solutions. Charge carriers transport charges from the interface to the liquid probe. When there are few carriers, the charge transfer rate is low, so the current value is low. As the number increases, the charge transportation occurs at a higher rate, and the current value increases. There is a saturation point where the number of carriers reaches a sweet spot: the charges are being transported at the highest rate without the carriers interfering with each other. A further increase in the number of carriers will result in the space in the liquid droplet being too crowded. Carriers carrying a charge going from the interface to the probe may bump into a returning carrier, and the returning carrier may “steal” the charge. It will take another delta response time for the returning carrier with the “stolen” charge to realize it is going in the wrong direction, turn around, and travel toward the probe. This aligns with the decreasing trend observed in the millimolar range with increasing ion concentration.

Figure 17 (a) and Figure 18 observe different current patterns collected between the oscilloscope and the biosensor box. This may be due to an internal capacitance at the biosensor's input pre-amplifier. Qualitatively, the charge generated at the interface gets deposited at the pre-amplifier, which blocks the signal from reaching the ADC port. In particular, the photoelectric steady-state response is blocked, which is observed on the oscilloscope. Connecting the pre-amplifier's output to the oscilloscope shows the waveform, which is a transient peak that decays almost instantly and stays at 0 while the LED is on. The peak goes through due to its relatively large magnitude. As the LED turns off, the pre-amplifier discharges and sends a negative signal to the ADC. Connecting the pre-amplifier to the oscilloscope displays the negative waveform. The question remains as

turning the LED off changes the temperature and generates a below-zero pyroelectric current peak regardless. Distinguishing the possible capacitor discharge from the negative transient requires some design not achieved. Notice that the feedback capacitor in the TIA exists to maintain stability by compensating for parasitic capacitance at the pre-amplifier's input node.

To recover the photoelectric current that disappeared at the output end of the pre-amplifier, there needs to be a way of either compensating the possible internal capacitance at its input or removing the pre-amplifier entirely and seeking other methods to measure the small current signal. Now, say, the capacitance is gone and the steady-state current due to the photoelectric effect is restored. The likely outcome is that the transient peaks will exhibit a different pattern across the concentration range since charging and discharging are no longer interfering with the reading.

Apart from the current patterns, the oscilloscope is also displaying current signals lower than the biosensor. This could be caused by the oscilloscope's input probes having a lower internal impedance than its nominal values. The load resistor and the oscilloscope's internal resistance divide the current generated at the interface, and more current flows into the measuring device than expected, causing the displayed voltage signal to be small.

Recall in Figure 18 that the unbiased NaCl (aq.)-silicon interface's transient current values collected with the biosensor box have two local peaks. This curve cannot be used as a reference to construct a concentration sensor since it associates one current signal value to multiple solution concentrations. The one-to-one correspondence occurs in specific narrow ranges. However, the 0.4 V forward-biased curve shown in Figure 18 (b) resolves the peak in the millimolar range. Going from 100 *mM* down to 10 μM , the transient current value changes monotonically, and these data points can help formulate a look-up table. The points in the range can be mapped using linear interpolation, and the sensor shall have a sensitivity at around 180 *nA* per decade, as listed in Table 3.

The capacitance measurement at the NaCl (aq.)-silicon interface shown in Figure 19 exhibits the same pattern as the unbiased transient current measurement using the biosensor box. Despite the difference in relative magnitudes, the matching positions of the local peaks between the blue and the red curves in Figure 19 suggest that the biosensor box's reading is directly affected by the capacitance of the device under test. The capacitance at the liquid-solid interface is likely due to the formation of an electrical double-layer, which is a phenomenon that occurs at the interface between an electronic solid surface and an electrolyte solution [34, 35]. It involves the separation of charges within the solution near the solid surface, resulting in a layered structure with distinct regions of positive and negative charges [34, 35]. As part of future work, the investigation may pay attention to the electrical double-layer formation at the NaCl (aq.)-silicon interface over concentrations and thus explore the reason behind observing a capacitance peak at 100 *nM*.

One potential way of resolving the peak at 100 *nM* is performing concentration detections with solution mixing. For instance, consider the 0.4 V forward-biased curve shown

in Figure 18 (b) as a reference. First, take a droplet from an unknown solution sample and measure the transient peak current value. Let it be r_1 . Then take another droplet from the sample and mix it with a droplet of 100 nM NaCl solution of the same volume, measure the transient peak current value again, and let it be r_2 . If r_2 is higher than r_1 by more than 150 nA, the sample's concentration is in the picomolar to low nanomolar range. If r_2 is higher than r_1 by less than 150 nA, the sample's concentration is in the high nanomolar range. If r_2 is less than r_1 , the sample's concentration is greater than 1 μ M. Although this method offers a detour to the nonlinearity in the current response, it is not practical. It requires users to perform the mixing procedure at a controlled ratio, which is prone to contamination. Hence, extending the concentration detection to the nanomolar range for NaCl solutions using the biosensor box remains a challenge.

5.2 TNF- α Cytokine Concentration Sensing and Future Works

As for measuring the TNF- α cytokine concentration based on the electric property change at the cytokine-aptamer interface, Figure 20 does not suggest a clear pattern that helps associate an electric current level with a cytokine concentration. This, together with the examination of the responses using the biosensor box, collects areas that warrant further investigation. Due to time constraints, this study does not explore the full extent of potential constructions and their impact on interfacial electric properties. Future experiments could focus on the systematic variation of contact configurations and the response's correlation with the cytokine-aptamer interface capacitance. These unexplored aspects of the biosensor's electric response present exciting opportunities for refinement toward TNF- α cytokine concentration detection.

Specifically, potential improvements exist in the setup used for collecting the pyroelectric and photoelectric current responses. The PDMS device constraining the liquid-solid interface area is mounted using tape, where a more reliable method of securing the PDMS would be bonding it to the silicon's surface. Joining the parts ensures no gap is left between them so that even for solutions with low surface tension, it would not seep and leak out of the PDMS well. The liquid contact is a probe tapping into the electrolyte. This configuration poorly defines the capacitance formed at the liquid-solid site. Instead of using a probe, the liquid contact may take the form of a plane. A copper plate and the silicon substrate could sandwich the solution droplet, and a wire coming out of the copper plate passes the signal generated at the interface to a measuring device. This configuration may produce a signal greater than the current construction, which could be handled by adjusting the gain at the pre-amplification stage accordingly.

References

- [1] W.M. Chu, Tumor Necrosis Factor, *Cancer Letters* 328 (2) (2013) 222-225.
- [2] C Popa, M. G. Netea, P. L.C.M. van Riel, J. W.M. van der Meer, A. F.H. Stalenhoef, The role of TNF- α in chronic inflammatory conditions, intermediary metabolism, and cardiovascular risk, *Journal of Lipid Research* 48 (4) (2007) 751-762.
- [3] K. J. Tracey, Y. Fong, D. G. Hesse, K. R. Manogue, A. T. Lee, G. C. Kuo, S. F. Lowry, A. Cerami, Anti-cachectin/TNF monoclonal antibodies prevent septic shock during lethal bacteraemia, *Nature* 330 (1987) 662-664.
- [4] Y. C. Cheong, J. B. Shelton, S. M. Laird, M. Richmond, G. Kudesia, T. C. Li, W. L. Ledger, IL-1, IL-6 and TNF- α concentrations in the peritoneal fluid of women with pelvic adhesions, *Human Reproduction* 17 (1) (2002) 69-75.
- [5] J. Zaremba, L. Losy, Early TNF- α levels correlate with ischaemic stroke severity, *Acta Neurologica Scandinavica* 104 (5) (2001) 288-295.
- [6] R. Ahmadi, A. Abnavi, H. Ghanbari, H. Mohandes, M. R. Mohammadzadeh, T. D. Silva, A. Hasani, M. Fawzy, F. Kabir, M. M. Adachi, Self-powered, broadband, and polarization-sensitive pyroelectric-photoelectric photodetector based on silicon-water heterojunction, *Nano Energy* 98 (2022) 107285.
- [7] M. Zheng, S. Lin, Z. Tang, Y. Feng, Z. L. Wang, Photovoltaic effect and tribovoltaic effect at liquid-semiconductor interface, *Nano Energy* 83 (2021) 105810.
- [8] P. Damas, A. Reuter, P. Gysen, J. Demonty, M. Lamy, P. Franchimont, Tumor necrosis factor and interleukin-1 serum levels during severe sepsis in humans, *Critical Care Medicine* 17 (10) (1989) 975-978.
- [9] V. S. Sastri, E. Ghali, M. Elboudjaini, Introduction and Principles of Corrosion, in *Corrosion Prevention and Protection*, John Wiley & Sons, 2007, pp. 20-28.
- [10] G. Song, A. Atrens, D. St John, X. Wu, J. Nairn, The anodic dissolution of magnesium in chloride and sulphate solutions, *Corrosion Science* 39 (10-11) (1997) 1981-2004.
- [11] H. Altun, S. Sen, Studies on the influence of chloride ion concentration and pH on the corrosion and electrochemical behaviour of AZ63 magnesium alloy, *Materials & Design* 25 (7) (2004) 637-643.
- [12] R. W. Whatmore, Pyroelectric Effects and Materials, *Rep. Prog. Phys.* 49 (1986) 1335-1386.

- [13] D. Zhang, H. Wu, C. R. Bowen, Y. Yang, Recent Advances in Pyroelectric Materials and Applications, *Small* 17 (2021) 2103960.
- [14] M.M. Yang, Z.D. Luo, Z. Mi, J. Zhao, S. Pei E, M. Alexe, Piezoelectric and pyroelectric effects induced by interface polar symmetry, *Nature* 584 (2020) 377-381.
- [15] D. Halliday, R. Resnick, K. S. Krane, Photoelectric Effect, in *Physics Vol. II*, 5th ed., John Wiley & Sons, 2002, pp. 1019-1021.
- [16] S. Klassen, The Photoelectric Effect: Reconstructing the Story for the Physics Classroom, *Science & Education* 20 (2011) 719-731.
- [17] M. F. Clark, R. M. Lister, M. Bar-Joseph, ELISA techniques, *Methods in Enzymology* 118 (1986) 742-766.
- [18] J. R. Crowther, Systems in ELISA, in *The ELISA Guidebook, Methods in Molecular Biology* 149, Humana Press, 2001, pp. 9-19.
- [19] BioLegend, ELISA MAXTM Deluxe Set Human TNF- α , biolegend.com, 2023. [Online]. Available: <https://www.biolegend.com/en-us/products/human-tnf-alpha-elisa-max-deluxe-2229>. [Accessed: Nov. 12, 2023].
- [20] BioLegend, Compare our ELISA Kits and Sets, biolegend.com, 2023. [Online]. Available: <https://www.biolegend.com/en-us/immunoassays/elisa/products>. [Accessed: Nov. 12, 2023].
- [21] ABCAM, Human TNF alpha ELISA Kit (ab181421), abcam.com, 2023. [Online]. Available: <https://www.abcam.com/products/elisa/human-tnf-alpha-elisa-kit-ab181421.html>. [Accessed: Nov. 12, 2023].
- [22] P. B. Lippa, L. J. Sokoll, D. W. Chan, Immunosensors – principles and applications to clinical chemistry, *Clinica Chimica Acta* 314 (1-2) (2001) 1-26.
- [23] L. Barhoumi, A. Baraket, F. G. Bellagambi, G. S. Karanasiou, M. B. Ali, D. I. Fotiadis, J. Bausells, N. Zine, M. Sigaud, A. Errachid, A novel chronoamperometric immunosensor for rapid detection for TNF- α in human saliva, *Sensors and Actuators B: Chemical* 266 (2018) 477-484.
- [24] M. Mazloum-Ardakani, L. Hosseinzadeh, A. Khoshroo, Label-free electrochemical immunosensor for detection of tumor necrosis factor α based on fullerene-functionalized carbon nanotubes/ionic liquid, *Journal of Electroanalytical Chemistry* 757 (2015) 58-64.

- [25] Great Lakes St. Lawrence Seaway System, Refractometer Information Sheet, greatlakes-seaway.com, 2019. [Online]. Available: https://greatlakes-seaway.com/wp-content/uploads/2019/10/may5th_refractometer_information_sheet.pdf. [Accessed: Nov. 12, 2023].
- [26] B. G. Streetman, S. K. Banerjee, Properties of Semiconductor Materials, in *Solid State Electronic Devices*, 7th ed., Pearson Education, 2015, pp. 560.
- [27] S. I. Raider, R. Flitsch, M. J. Palmer, Oxide Growth on Etched Silicon in Air at Room Temperature, *Journal of the Electrochemical Society* 122 (3) (1975) 2134225.
- [28] Texas Instruments, TL074 General-purpose op amps, ti.com, 2023. [Online]. Available: <https://www.ti.com/product/TL074>. [Accessed: Nov. 12, 2023].
- [29] STMicroelectronics, STM32L432KC, st.com, 2023. [Online]. Available: <https://www.st.com/en/microcontrollers-microprocessors/stm32l432kc.html>. [Accessed: Nov. 12, 2023].
- [30] Mornsun Power, MORNSUN DC/DC-Fixed Input Converter IA0505S-1WR3, mornsun-power.com, 2022. [Online]. Available: <https://www.mornsun-power.com/index/sitesearch/partlink/keyword/IA0505S-1WR3.html>. [Accessed: Nov. 12, 2023].
- [31] DigiKey, Products, digikey.ca, 2023. [Online]. Available: <https://www.digikey.ca/en/products>. [Accessed: Nov. 12, 2023].
- [32] STMicroelectronics, STM32L4 – ADC Product Training, st.com, 2023, [Online]. Available: https://www.st.com/resource/en/product_training/stm32l4_analog_adc.pdf. [Accessed: Nov. 12, 2023].
- [33] Tektronix, MDO3000 Series Mixed Domain Oscilloscope, tek.com, 2023. [Online]. Available: https://download.tek.com/document/48W_30076_0_HR.pdf. [Accessed: Nov. 12, 2023].
- [34] W. Schmickler, Electronic Effects in the Electric Double Layer, *Chem. Rev.* 96 (8) (1996) 3177-3200.
- [35] R. Parsons, The electrical double layer: recent experimental and theoretical developments, *Chem. Rev.* 90 (5) (1990) 813-826.

Appendix A: NaCl Solution Preparation

Objective:

To obtain NaCl solutions with concentrations ranging from picomolar to millimolar.

Materials:

- NaCl crystal
- Deionized (DI) water
- Weight balance
- Wax-glazed weighing paper
- Spatula
- Glass vials
- Vial stand
- Transfer pipette
- Micropipette
- Vortex mixer

Procedures:

1. Knowing the molar mass of NaCl is 58.44 g/mol , a 1-molar NaCl solution can be obtained by dissolving 0.5844 g of NaCl crystal in 10 mL of DI water.
2. Close the vial and hold it against a vortex mixer. Spin mix for 30 seconds.
3. Repeat the dilution recursively to obtain solutions with the assorted concentrations. Refer to the following table for proportions. Notice the 0-molar NaCl solution is DI water.

Table 4. NaCl solution dilution ratios.

Goal Concentration	Source	DI (μL)	End volume (μL)
100 mM	100 μL of 1 M	900	1000-100=900
10 mM	100 μL of 100 mM	900	1000-100=900
1 mM	100 μL of 10 mM	900	1000-100=900
100 μM	100 μL of 1 mM	900	1000-100=900
10 μM	100 μL of 100 μM	900	1000-100=900
1 μM	100 μL of 10 μM	900	1000-100=900
100 nM	100 μL of 1 μM	900	1000-100=900
10 nM	100 μL of 100 nM	900	1000-100=900
1 nM	100 μL of 10 nM	900	1000-100=900
100 pM	100 μL of 1 nM	900	1000-100=900
10 pM	100 μL of 100 pM	900	1000-100=900
1 pM	100 μL of 10 pM	900	1000
0 M	DI water	1000	1000

Appendix B: TNF- α Cytokine Protein Solution Preparation

Objective:

To obtain TNF- α cytokine protein solutions with concentrations ranging from femtomolar to nanomolar.

Materials:

- TNF- α cytokine protein
- Phosphate-buffered saline (PBS)
- 0.5 mL vials
- Vial stand
- Micropipette
- Vortex mixer

Procedure:

1. Dim the room light to reduce protein's light exposure during solution transfer.
2. Take a cytokine protein vial from the fridge and leave it on a stand to defrost.
3. Notice a vial contains 20 μL of cytokine at 23 $\mu\text{g}/\text{mL}$. Add 72 μL of PBS to dilute the concentration to 5 $\mu\text{g}/\text{mL}$, corresponding to 300 nM .

TNF- α has a molecular mass of 17.3 kDa , corresponding to 17.3 kg/mol .

$$\frac{5 \mu\text{g}}{1 \text{mL}} \cdot \frac{1 \text{mol}}{17.3 \text{kg}} = \frac{5 \cdot 10^{-6}}{10^{-3} \cdot 17.3 \cdot 10^3} \cdot \frac{\text{mol}}{\text{L}} = 289 \text{nM}.$$

Add PBS:

$$20 \cdot \frac{23}{5} = 92, 92 - 20 = 72 \mu\text{L}.$$

4. Close the vial and hold it against a vortex mixer. Spin mix for 30 seconds.
5. Repeat the dilution recursively to obtain solutions with the assorted concentrations. Refer to the following table for proportions. Notice the 0-molar cytokine protein solution is PBS.

Table 5. TNF- α solution dilution ratios.

Goal Concentration	Source	PBS (μL)	End volume (μL)
100 nM	68 μL of 300 nM	132	200-20=180
10 nM	20 μL of 100 nM	180	200-20=180
1 nM	20 μL of 10 nM	180	200-20=180
100 pM	20 μL of 1 nM	180	200-20=180
10 pM	20 μL of 100 pM	180	200-20=180
1 pM	20 μL of 10 pM	180	200-20=180
100 fM	20 μL of 1 pM	180	200-20=180
10 fM	20 μL of 100 fM	180	200-20=180
1 fM	20 μL of 10 fM	180	200
0 M		200	200

Appendix C: Aptamer-Functionalization on an N-type Silicon Substrate with 5 nm of Aluminum Oxide Coating

Objective:

To functionalize a 5nm-Al₂O₃-coated n-type silicon substrate with fluorescent aptamers. To check for surface functionalization quality under a laser.

Materials:

- Al₂O₃ coated silicon substrate
- TNF- α fluorescent aptamer
- (3-Aminopropyl)triethoxysilane 99% (APTES)
- Glutaraldehyde (GA), 25% in H₂O
- Isopropanol (IPA)
- 100% ethanol
- Deionized (DI) water
- Molecular biology grade (MBG) water
- Phosphate-buffered saline (PBS)
- Diamond pen
- Tweezers
- Transfer pipette
- Syringe
- Glass vial
- Aluminum foils
- Nitrogen or Argon compressed gas tank
- Fridge/freezer
- Hot plate
- Blue laser
- Filter goggles 180-532 nm OD 7+ 48%VLT

Procedures:

1. Silicon Preparation
 - 1.1. Reserve a small area on the silicon surface for solid contact and scratch the oxide coating with a diamond tip pen.
 - 1.2. Rinse the substrate with acetone, IPA, and DI water.
2. Plant the APTES Linkers
 - 2.1. Add the following materials into a glass vial: 9.5 mL of 100% ethanol, 0.5 mL of DI water, and 0.1 mL of APTES. Use a pipette for large volume of liquid transfer and a syringe for small volume.
 - 2.2. Mix the APTES solution gently and divide the solution into vials depending on the number of substrates to be functionalized.
 - 2.3. Place silicon substrates into the solution vials with the desired side facing up. Ensure the substrates are fully submerged.
 - 2.4. Close the vial caps and leave for 45 minutes.
 - 2.5. Take the substrates out of the APTES solutions with a tweezer and rinse the substrates with IPA.
 - 2.6. Blow dry the substrates with N₂ or Ar gas.
 - 2.7. Bake the substrates on a hot plate at 155 degrees Celsius for 5 minutes. Remove the substrates from the hot plate and let them cool.

3. Plant the GA Linkers
 - 3.1. Add the following materials into a glass vial using transfer pipettes: 2 *mL* of DI water, 2.5 *mL* of PBS, and 0.5 *mL* of GA.
 - 3.2. Mix the GA solution gently and divide the solution into vials depending on the number of substrates to be functionalized.
 - 3.3. Place silicon substrates into the solution vials with the desired side facing up. Ensure the substrates are fully submerged. Notice the solution exhibits a relatively high surface tension, that the substrates tend to float on the surface. Use a tweezer to help with submerging the substrates.
 - 3.4. Close the vial caps and leave for 2 hours.
 - 3.5. Take the substrates out of the GA solutions with a tweezer and rinse the substrates with PBS.
 - 3.6. Blow dry the substrates with N₂ or Ar gas. Turn the nozzle to give a relatively high gas pressure and blow the droplet off the surface quickly. Minimize the amount of residue left on the surface.

4. Plant the Aptamers
 - 4.1. Dilute 100 μL of TNF- α fluorescent aptamer solution with 1.4 *mL* of PBS. Additional PBS may be added up to 0.5 *mL* to make 2 *mL* of diluted aptamer solution.
 - 4.2. Mix the aptamer solution gently and divide the solution into vials depending on the number of substrates to be functionalized.
 - 4.3. Place silicon substrates into the solution vials with the desired side facing up. Again, ensure the substrates are fully submerged as the substrates tend to float on the surface.
 - 4.4. Wrap the vials tightly with aluminum foils.
 - 4.5. Place the vials in a cabinet (a dark place) at room temperature and leave overnight.
 - 4.6. Take the substrates out of the aptamer solutions and rinse the substrates with MBG water.
 - 4.7. Blow dry the substrates.

5. Functionalization check and storage
 - 5.1. Shine the substrates surface with a blue laser and observe for green illumination. Successful functionalization is indicated by a green spot as the fluorescent aptamers absorb blue light and emit green light.
 - 5.2. When the substrates are not in use, store them in glass vials wrapped with aluminum foils and keep them cold in a freezer such that the proteins will not degrade.

Appendix D: PDMS Mixing, Degassing, and Baking

Objective:

To make the PDMS square well that will be mounted on a silicon substrate, constraining the liquid-solid interface area.

Materials:

- PDMS base and cure agent
- 3D-printed mold
- Weight balance
- Boat/Petri dish
- Transfer Pipette
- Stirring rod
- Wiping tissue
- Vacuum chamber
- Aluminum foil
- Oven

Procedure:

1. Mix and Stir
 - 1.1 Place a weight boat/dish on a weight balance and tare.
 - 1.2 Use a pipette to transfer an appropriate amount of PDMS base (e.g., 10 g) into the weight boat. Notice the PDMS base is high in viscosity. Squeeze and release the end of the pipette slowly such that the liquid on the inner side of the pipette can flow.
 - 1.3 Tare the weight balance and use a new pipette to add the PDMS cure (e.g., 1 g) into the weight boat. The ratio between the base and the cure should be 10:1.
 - 1.4 Stir and mix the base and the cure for 3 minutes.
2. Degas
 - 2.1 Place some aluminum foil on the bottom of the vacuum chamber to catch any possible splashing.
 - 2.2 Place the boat/dish containing the PDMS in the vacuum chamber and close the chamber lid.
 - 2.3 Ensure the valve is sealed well and turn the vacuum pump on. Let the PDMS degas for 15 minutes.
 - 2.4 Slowly open the valve to let the air in. Opening the valve quickly would create strong wind in the chamber, which will likely splash the PDMS. Remove the plug at the tip of the valve and open the chamber.
3. Mold and Cast
 - 3.1 Take the PDMS-containing boat out of the vacuum chamber.
 - 3.2 Use a pipette to slowly transfer the PDMS from the boat to the mold. Try to minimize the amount of air bubbles introduced during the transferring process.
 - 3.3 Place the PDMS-containing molds into a new Petri dish. Degas the PDMS again if necessary.
 - 3.4 Bake the PDMS in an oven at 60 degrees Celsius for 2 hours.

Appendix E: List of Biosensor Box PCB Component Footprints

Table 6. Biosensor Box PCB component footprints.

Part name	Footprint	Purchase Link
R1; 2M0	Resistor_SMD: R_1206_3216Metric_Pad_1.30x1.75mm_HandSolder	https://www.digikey.ca/en/products/detail/yageo/RC1206FR-072ML/728613
R2, R3; 40k0	Resistor_SMD: R_1206_3216Metric_Pad_1.30x1.75mm_HandSolder	https://www.digikey.ca/en/products/detail/yageo/RT1206BRD0740KL/5936957
C1; 10p0, 16V	Capacitor_SMD: C_0805_2012Metric_Pad_1.18x1.45mm_HandSolder	https://www.digikey.ca/en/products/detail/w%C3%BCrth-elektronik/885012007010/5453669
C2, C3; 10n0, 10V	Capacitor_SMD: C_0805_2012Metric_Pad_1.18x1.45mm_HandSolder	https://www.digikey.ca/en/products/detail/w%C3%BCrth-elektronik/885012207011/5453876
C4, C5, C6; 4u7, 16V	Capacitor_SMD: C_0805_2012Metric_Pad_1.18x1.45mm_HandSolder	https://www.digikey.ca/en/products/detail/samsung-electro-mechanics/CL21A475KOFNNNE/3886723
C7, C9; 10u0, 25V	Capacitor_SMD: C_0805_2012Metric_Pad_1.18x1.45mm_HandSolder	https://www.digikey.ca/en/products/detail/samsung-electro-mechanics/CL21A106KAYNNNE/3890977
C8, C10; 100n0, 10V	Capacitor_SMD: C_0805_2012Metric_Pad_1.18x1.45mm_HandSolder	https://www.digikey.ca/en/products/detail/kyocera-avx/KGM21NR71A104KT/1545111
D1; LED	LED_THT: LED_D5.0mm_Clear	https://www.digikey.ca/en/products/detail/tt-electronics-optek-technology/ovlgc0c6b9/827121
PS1; IA0505S	Converter_DCDC: Converter_DCDC_XP_POWER-IAxxxxS_THT	https://www.digikey.ca/en/products/detail/mornsun-america-llc/A0505S-1WR3/13168392
U1; TL074	Package_SO: SOIC-14_3.9x8.7mm_P1.27mm	https://www.digikey.ca/en/products/detail/texas-instruments/TL074HIDR/13563033
U2; STM32 pins	Connector_PinSocket_2.54mm: PinSocket_1x15_P2.54mm_Vertical	https://www.digikey.ca/en/products/detail/sullins-connector-solutions/PPP_C031LFBN-RC/810175
U3; sensor probes (current source)	Connector_PinSocket_2.54mm: PinSocket_1x2_P2.54mm_Vertical	https://www.digikey.ca/en/products/detail/sullins-connector-solutions/PPT_C021LFBN-RC/810142

Appendix F: Biosensor PCB Front and Back Copper Layers, and PCB Printing Specification

Only the front and back copper layers are shown below in Figure 21 because the solder paste layers, the silkscreen on the two sides, and the solder masks are trivial after the connections are laid out.

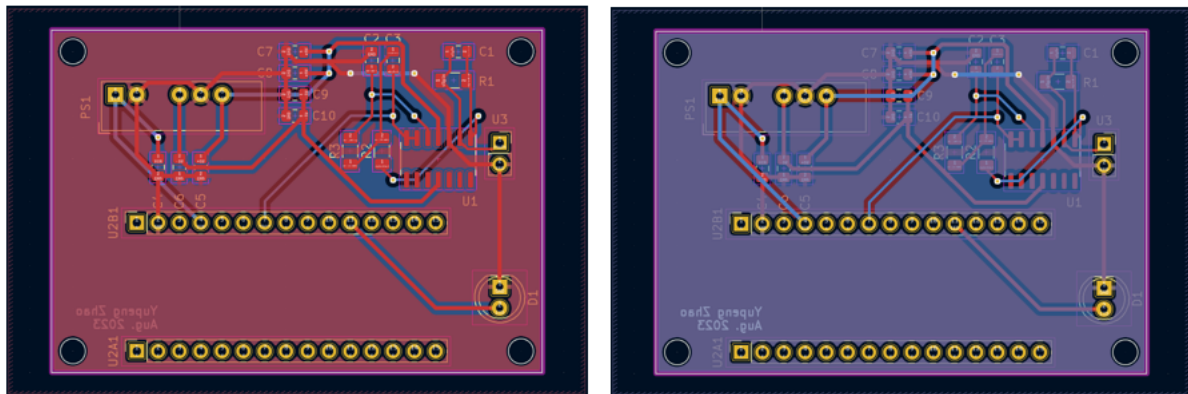


Figure 21. Front copper layer (left) and back copper layer (right).

Table 7. PCB printing specifications.

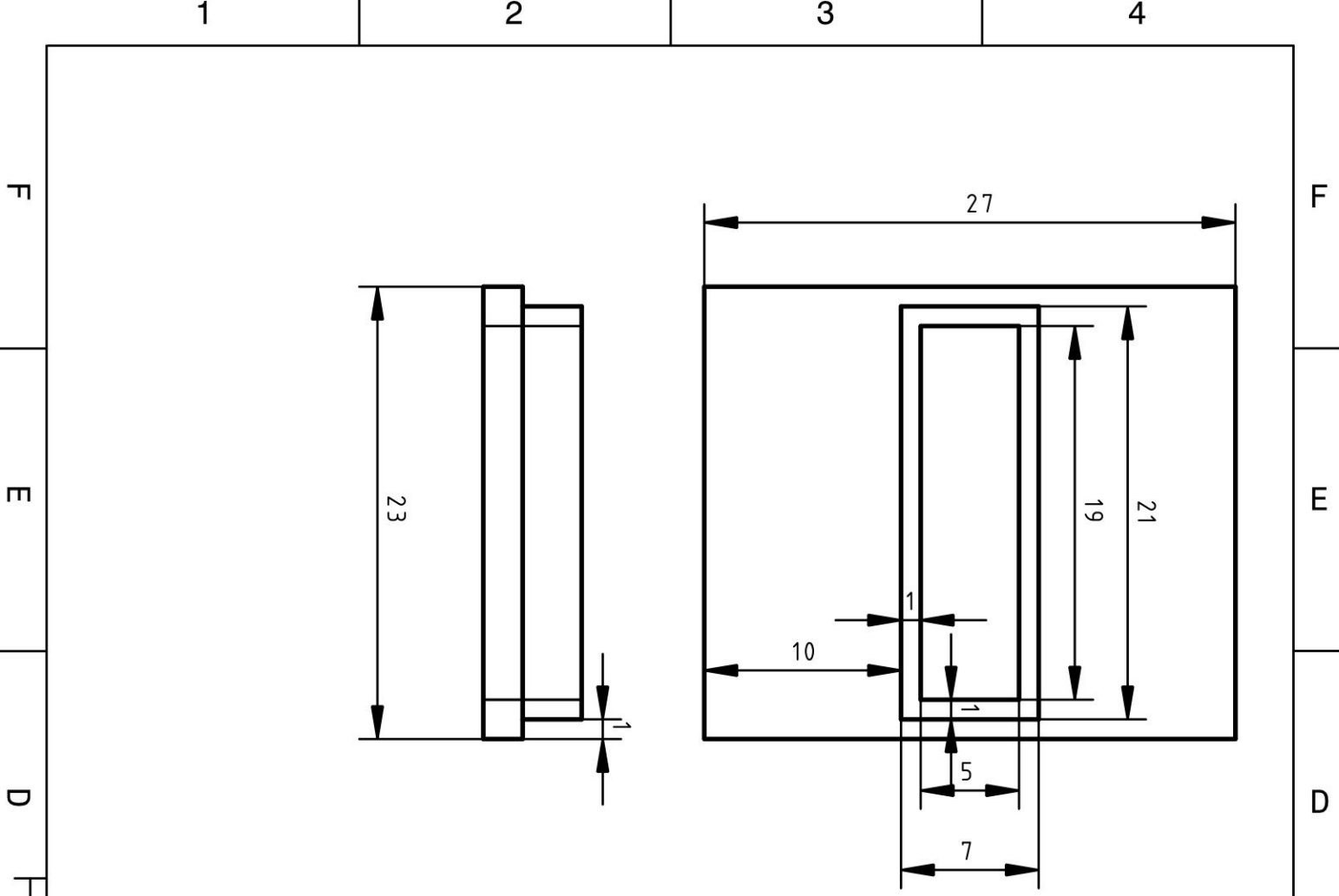
Base Material: FR-4	Appearance Quality: IPC Class 2 Std
Dimension: 58.4 mm* 40.6 mm	Silkscreen: Ink-jet/Screen Printing
Impedance Control: No	Board Outline Tolerance: ± 0.2 mm
PCB Color: Green	Layers: 2
Via Covering: Tended	PCB Thickness: 1.6
Deburring/Edge Rounding: No	Silkscreen: White
Gold Fingers: No	Surface Finish: HASL (with lead)
Castellated Holes: No	Outer Copper Weight: 1 oz

Appendix G: List of 3D-printed Parts, Projection views, and Dimensions³

The following pages display the projection views of the 3D-printed parts in the order as they are listed:

- PDMS mold side piece
- PDMS mold bottom piece
- Biosensor box base
- Biosensor box substrate holder
- Biosensor box lid
- Biosensor box liquid probe holder
- Biosensor box solid probe holder
- Biosensor box LED holder
- Biosensor box square stand 32-0
- Biosensor box square stand 4-0
- Biosensor box square washer 0-5

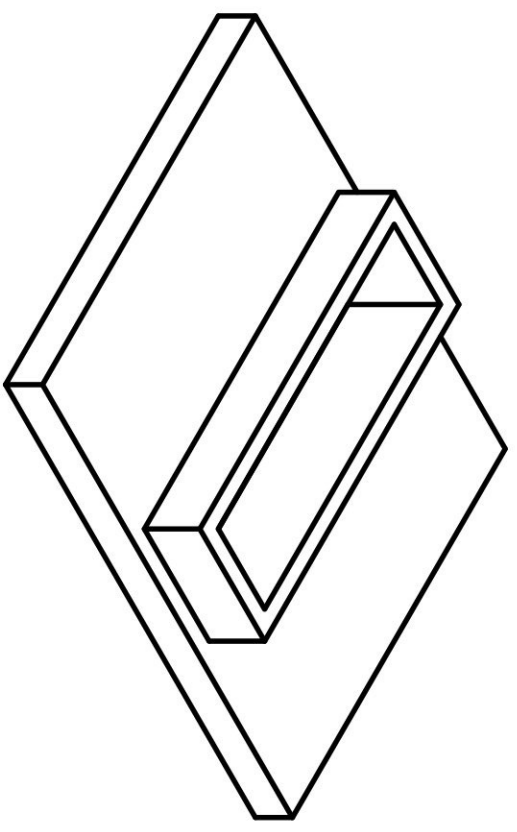
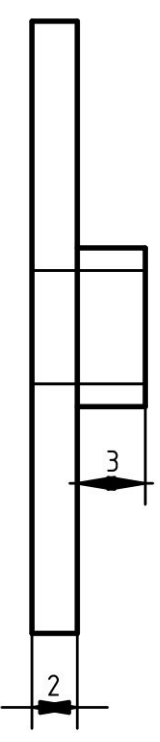
³ All dimensions are in millimeters.



DESIGNED BY: Yupeng Zhao		PDMS Mold 3D Parts	
DATE: 2023/05/31		Mold Side Piece	
SIZE A4	WEIGHT (kg)	DRAWING NUMBER	SHEET 1/2
SCALE			
This drawing is our property; it can't be reproduced or communicated without our written consent.			

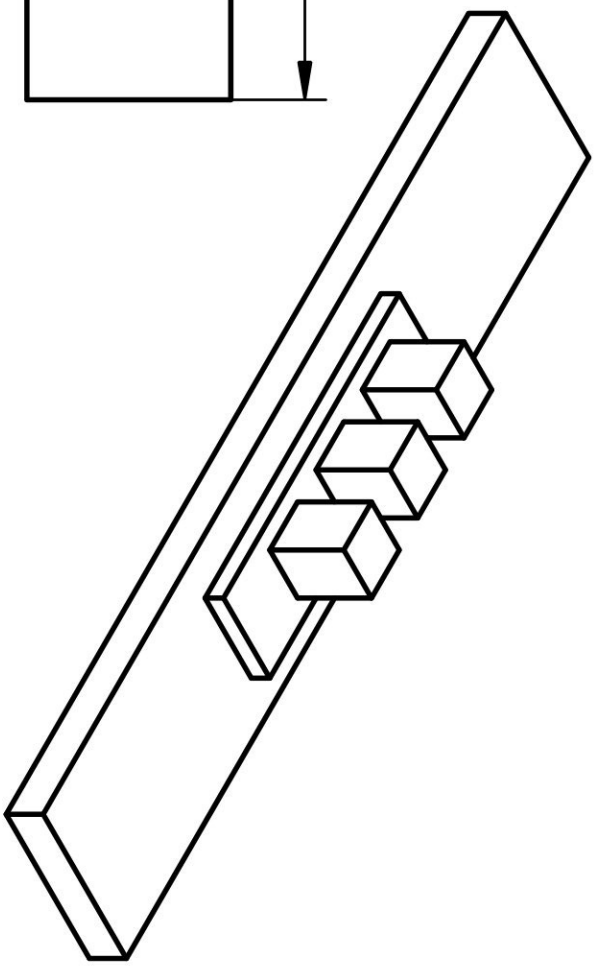
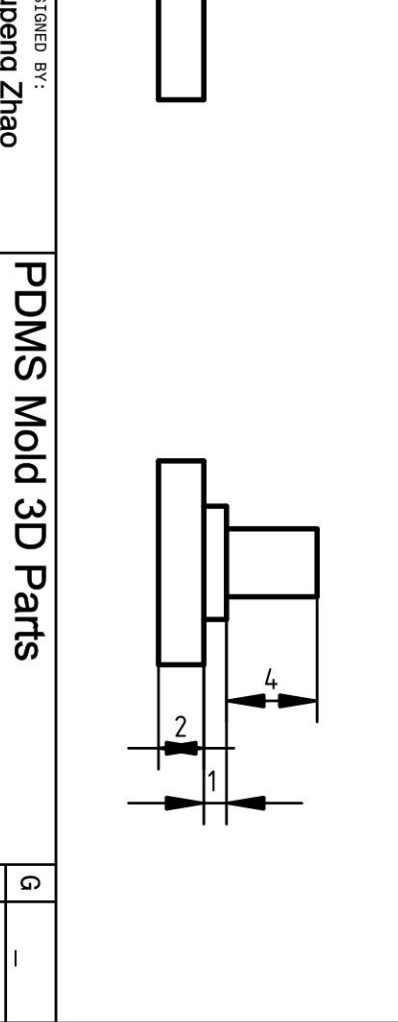
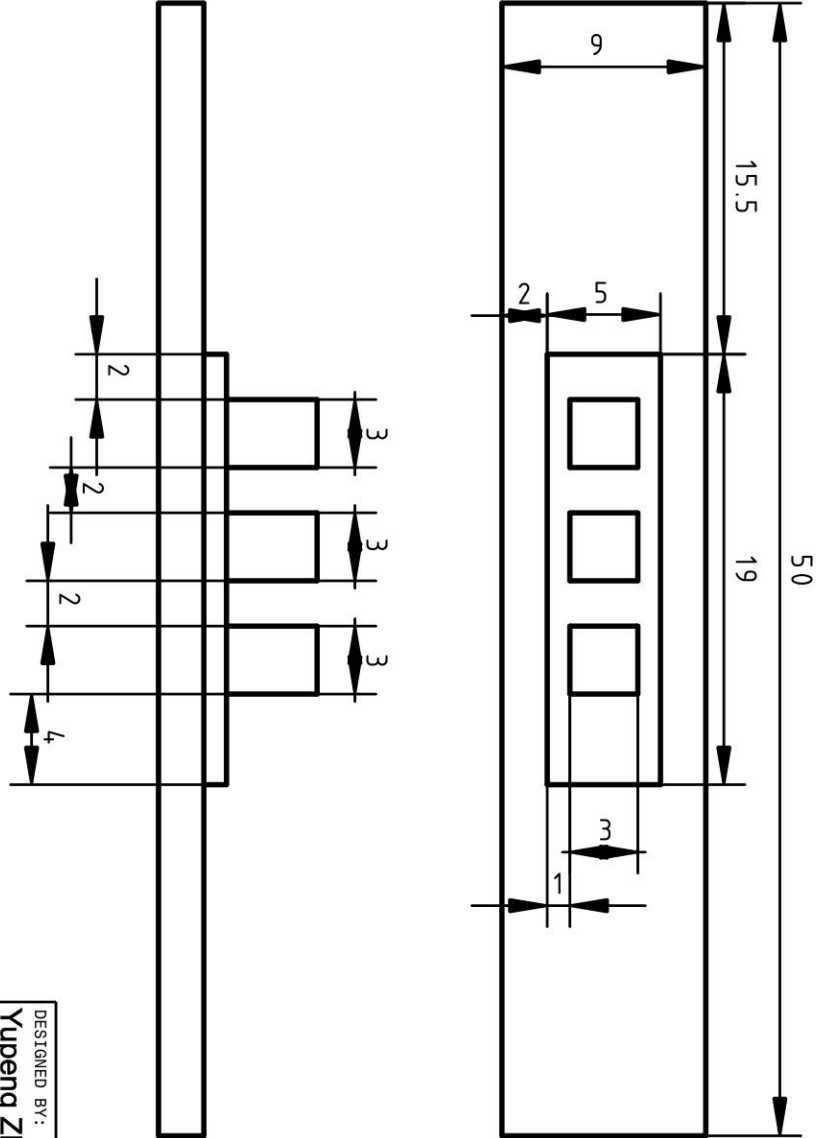
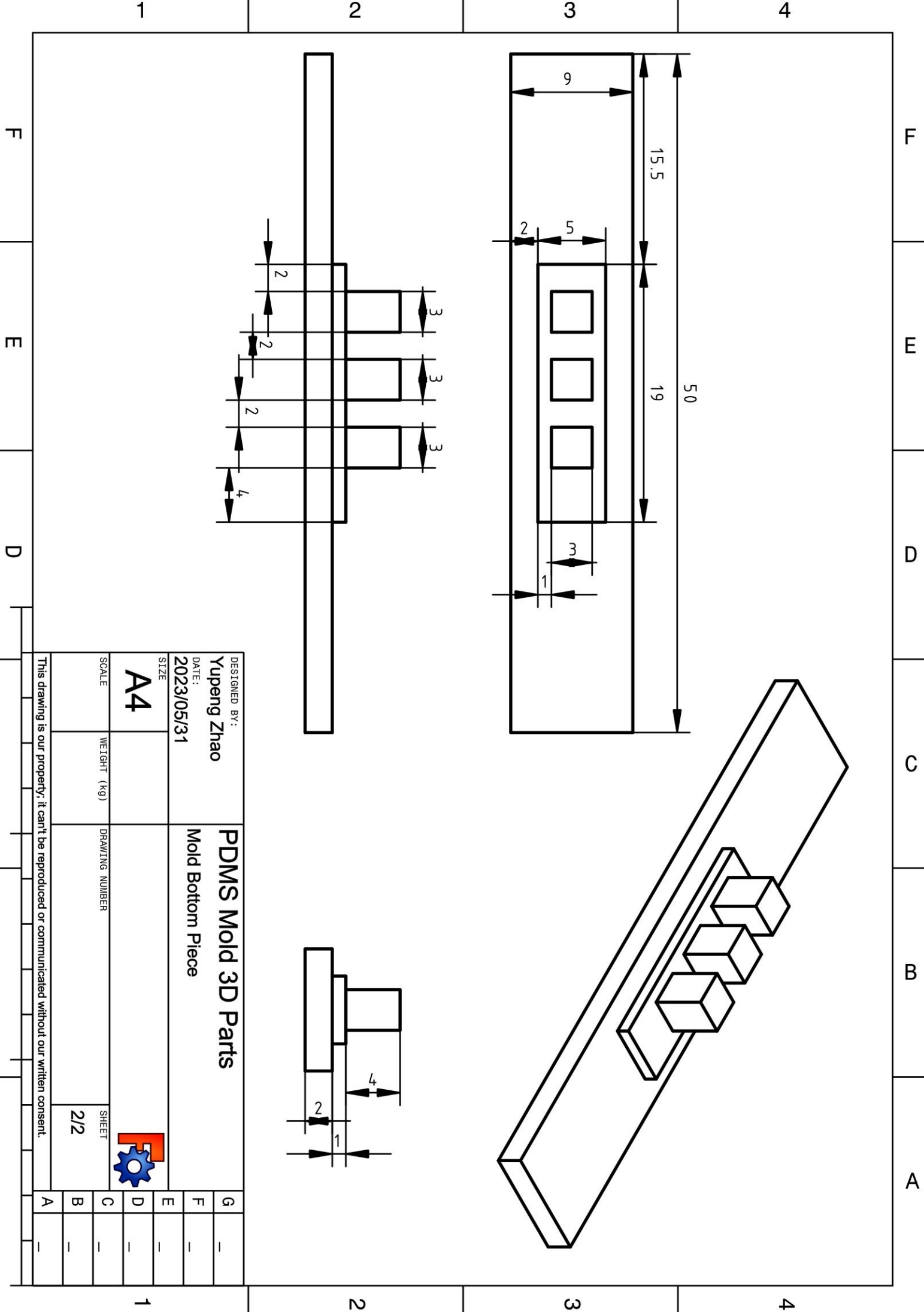


G	1
F	-
E	-
D	-
C	-
B	-
A	-



1 2 3 4

F E D C B A



DESIGNED BY:
Yupeng Zhao

DATE:
2023/05/31

PDMS Mold 3D Parts
Mold Bottom Piece

SIZE
A4

SCALE WEIGHT (kg) DRAWING NUMBER

SHEET
2/2



This drawing is our property; it can't be reproduced or communicated without our written consent.

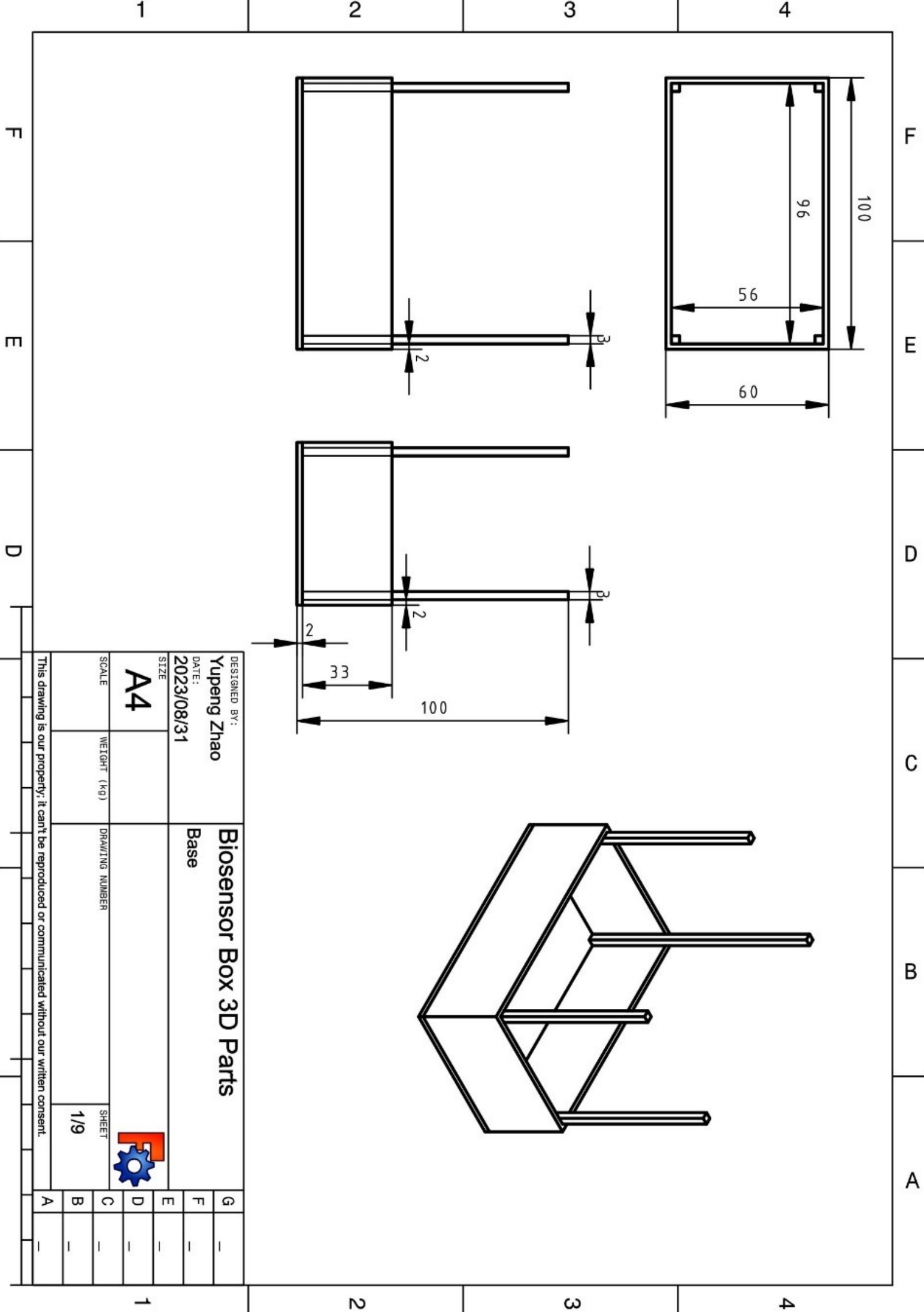
G	-
F	-
E	-
D	-
C	-
B	-
A	-

1

2

3

4



DESIGNED BY:
Yupeng Zhao
 DATE:
 2023/08/31

Biosensor Box 3D Parts
 Base

SIZE
A4

SCALE

WEIGHT (kg)

DRAWING NUMBER

SHEET



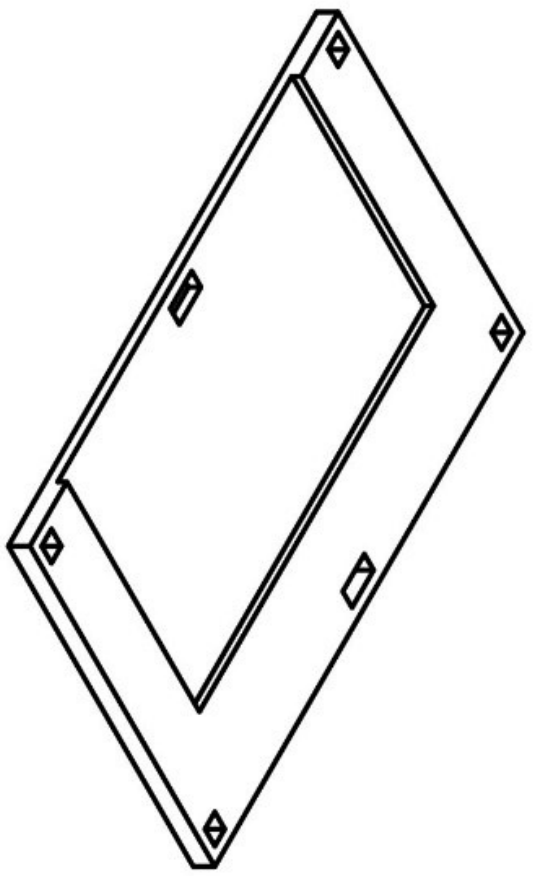
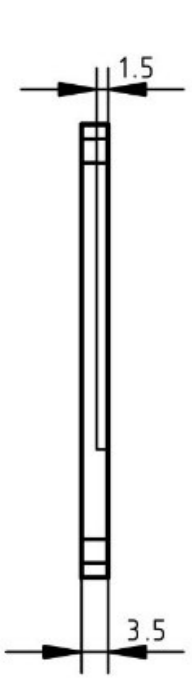
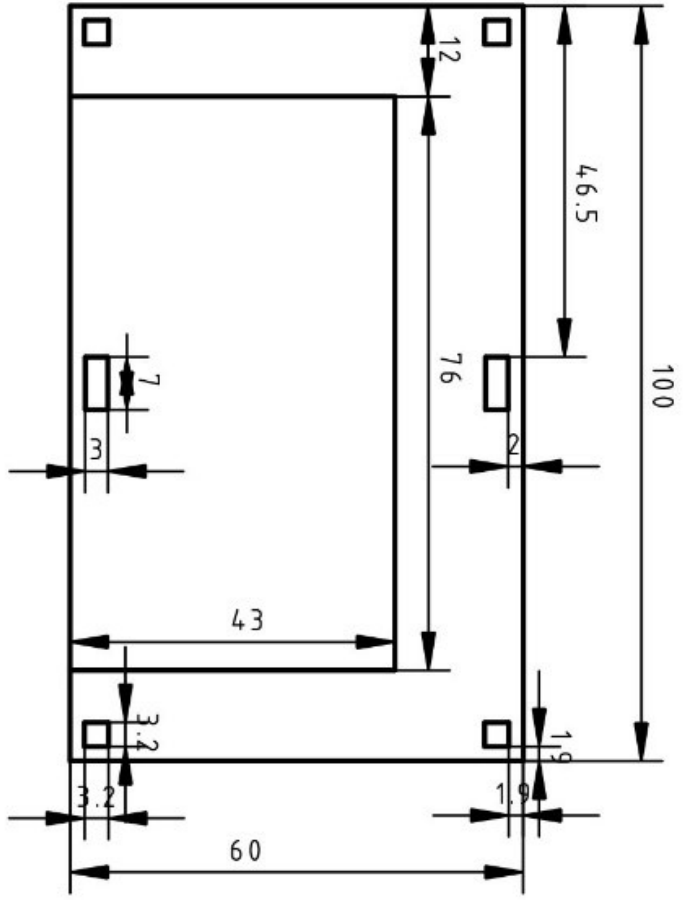
1/9

This drawing is our property. It can't be reproduced or communicated without our written consent.

G	—	1
F	—	1
E	—	1
D	—	1
C	—	1
B	—	1
A	—	1

1 2 3 4

F E D C B A

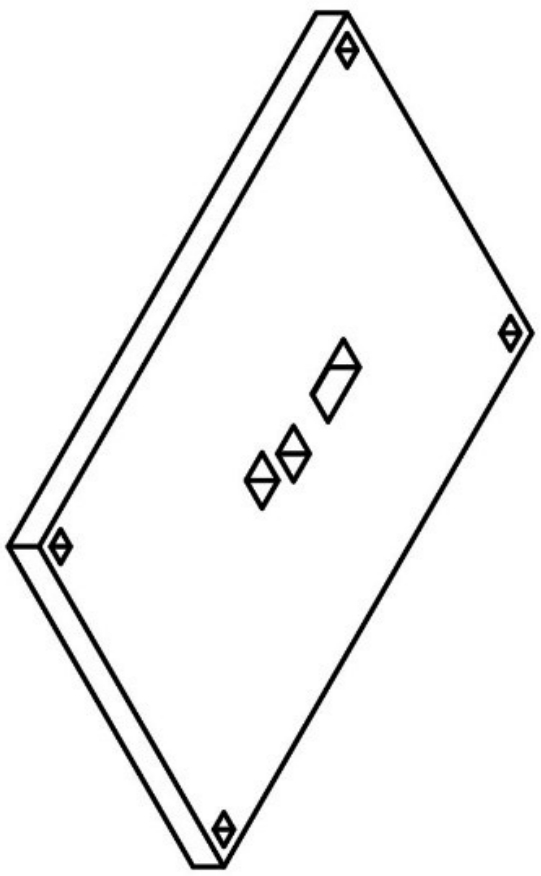
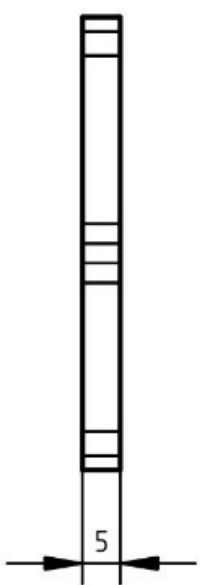
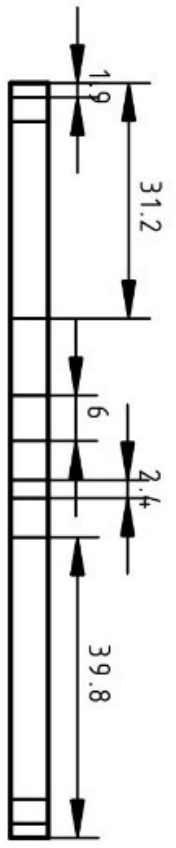
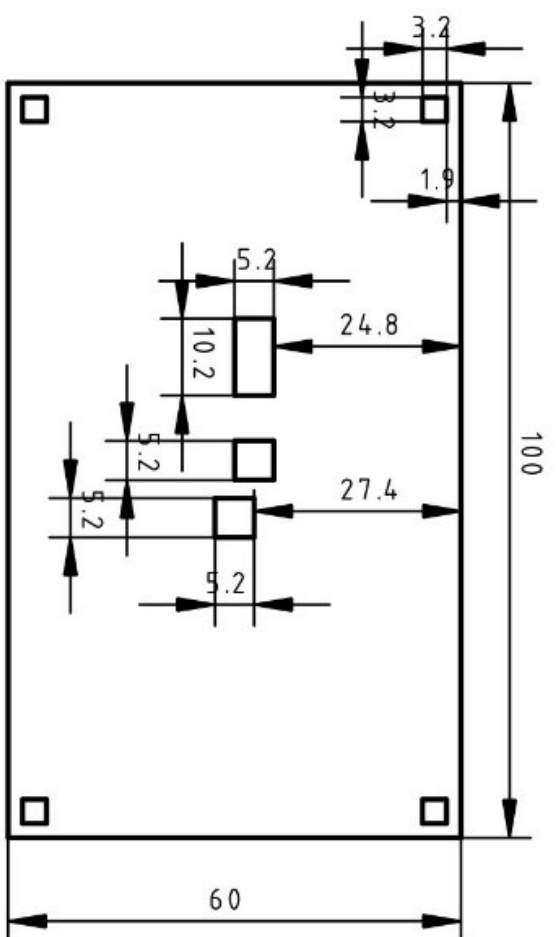


F E D

DESIGNED BY: Yupeng Zhao	Biosensor Box 3D Parts		G
DATE: 2023/08/03	Substrate holder		F
SIZE A4			E
SCALE	WEIGHT (kg)	DRAWING NUMBER	D
			C
		SHEET 2/9	B
This drawing is our property; it can't be reproduced or communicated without our written consent.			A



1 2 3 4



F E D

F E D C B A

1

2

3

4

1

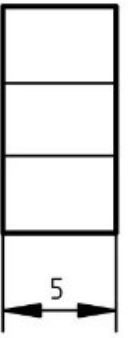
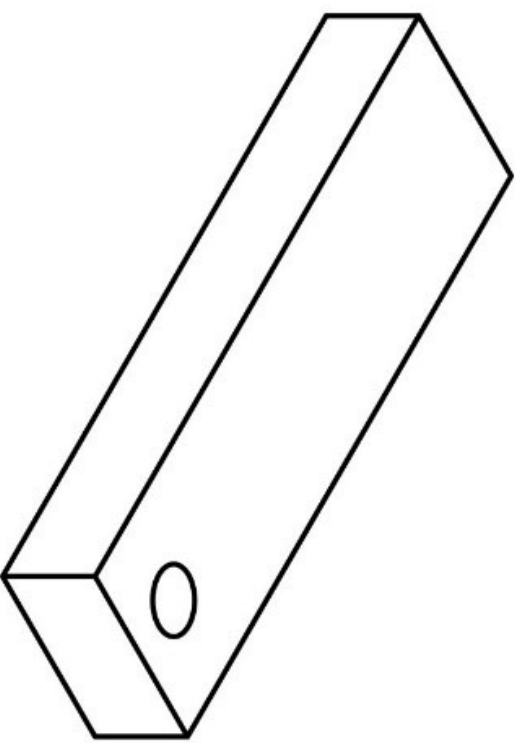
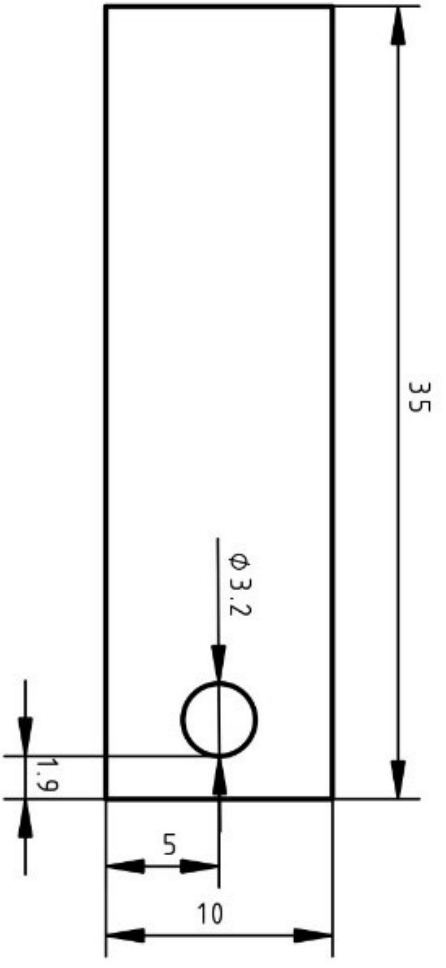
2

3

4

DESIGNED BY: Yupeng Zhao		DRAWING NUMBER		SHEET	
DATE: 2023/08/31		Lid		3/9	
SIZE A4		DRAWING NUMBER		SHEET	
SCALE		WEIGHT (kg)		3/9	
This drawing is our property. It can't be reproduced or communicated without our written consent.					
G	-	G	-	G	-
F	-	F	-	F	-
E	-	E	-	E	-
D	-	D	-	D	-
C	-	C	-	C	-
B	-	B	-	B	-
A	-	A	-	A	-





1

2

3

4

F

E

D

F

E

D

C

B

A

DESIGNED BY:
Yupeng Zhao
DATE:
2023/08/31

Biosensor Box 3D Parts
Liquid Probe Support



SIZE
A4

SCALE

WEIGHT (kg)

DRAWING NUMBER

SHEET
4/9

This drawing is our property; it can't be reproduced or communicated without our written consent.

G

F

E

D

C

B

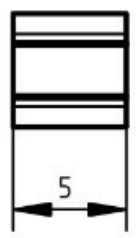
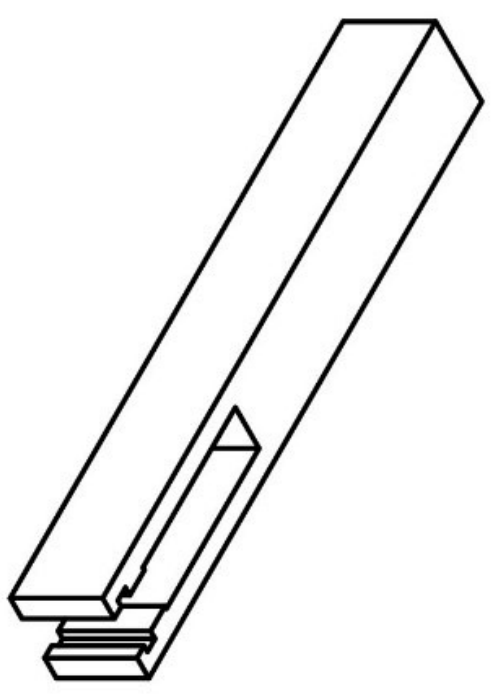
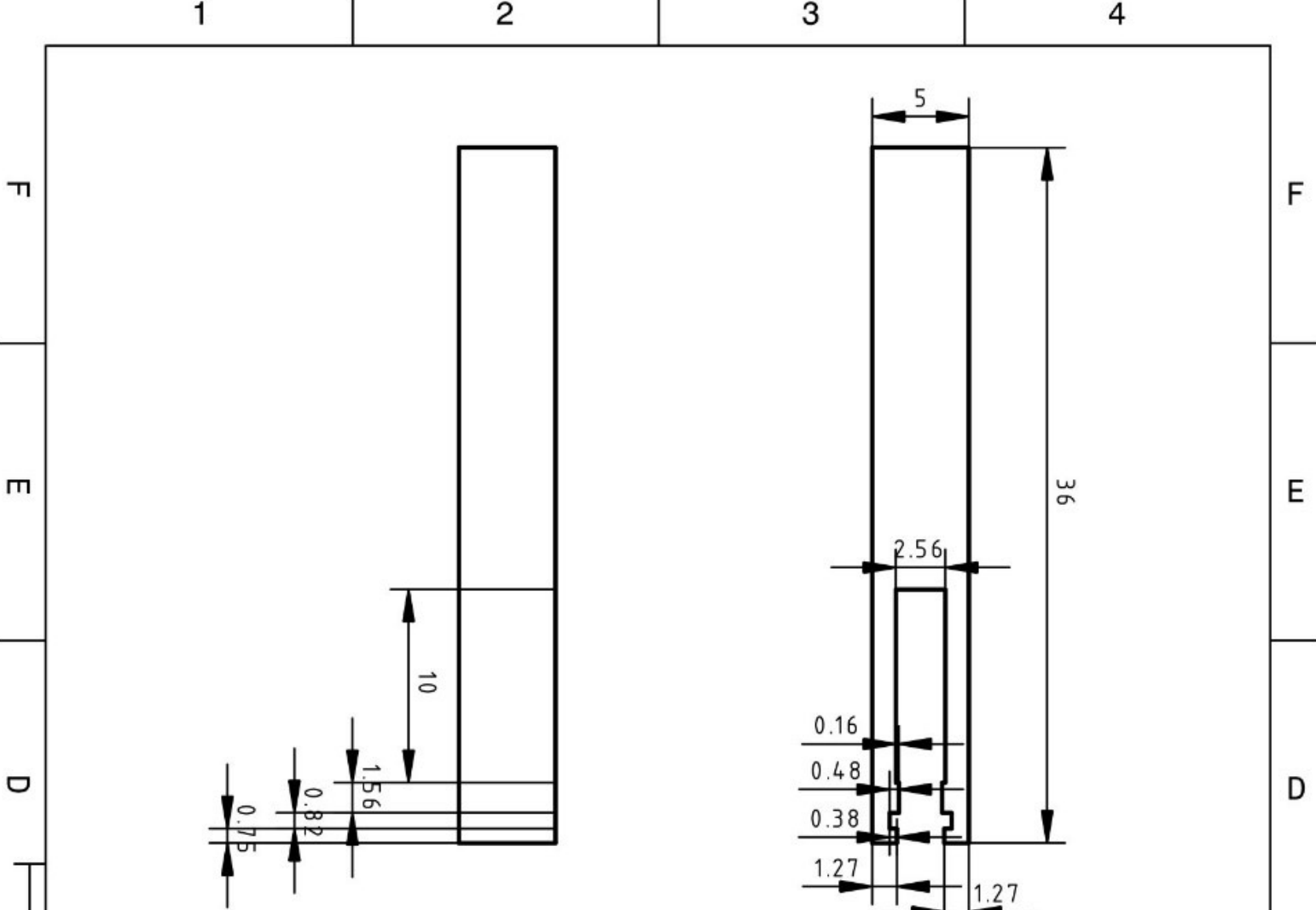
A

1

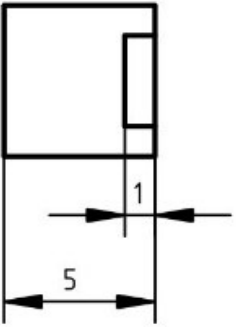
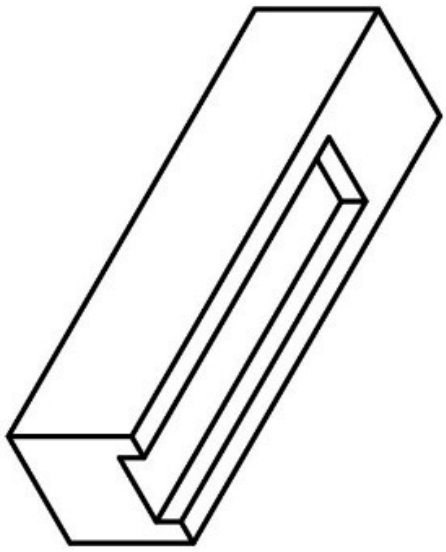
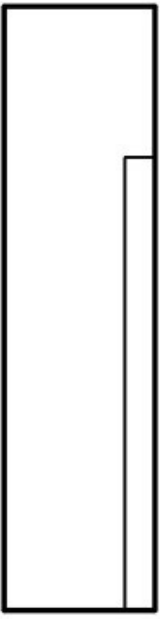
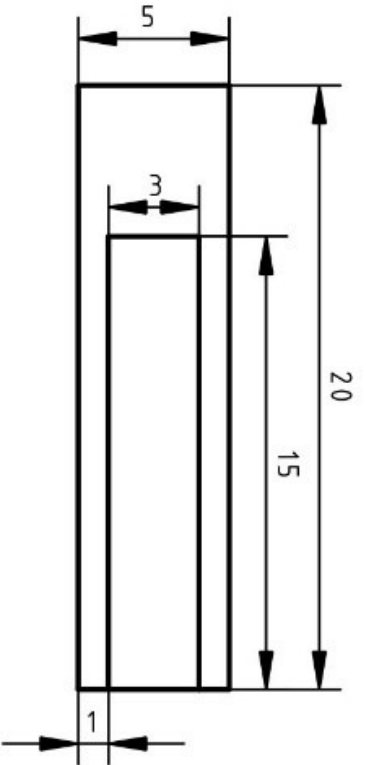
2

3

4

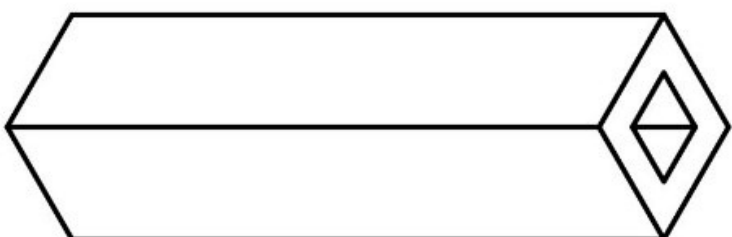
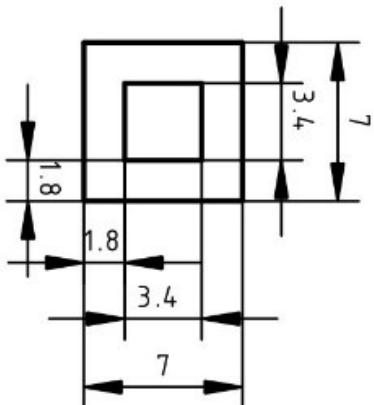
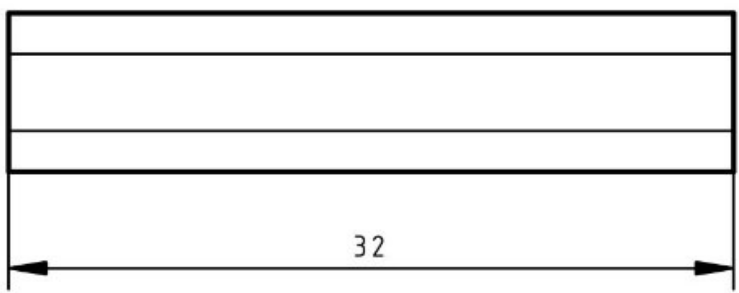
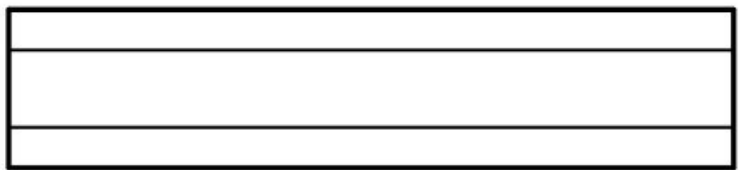
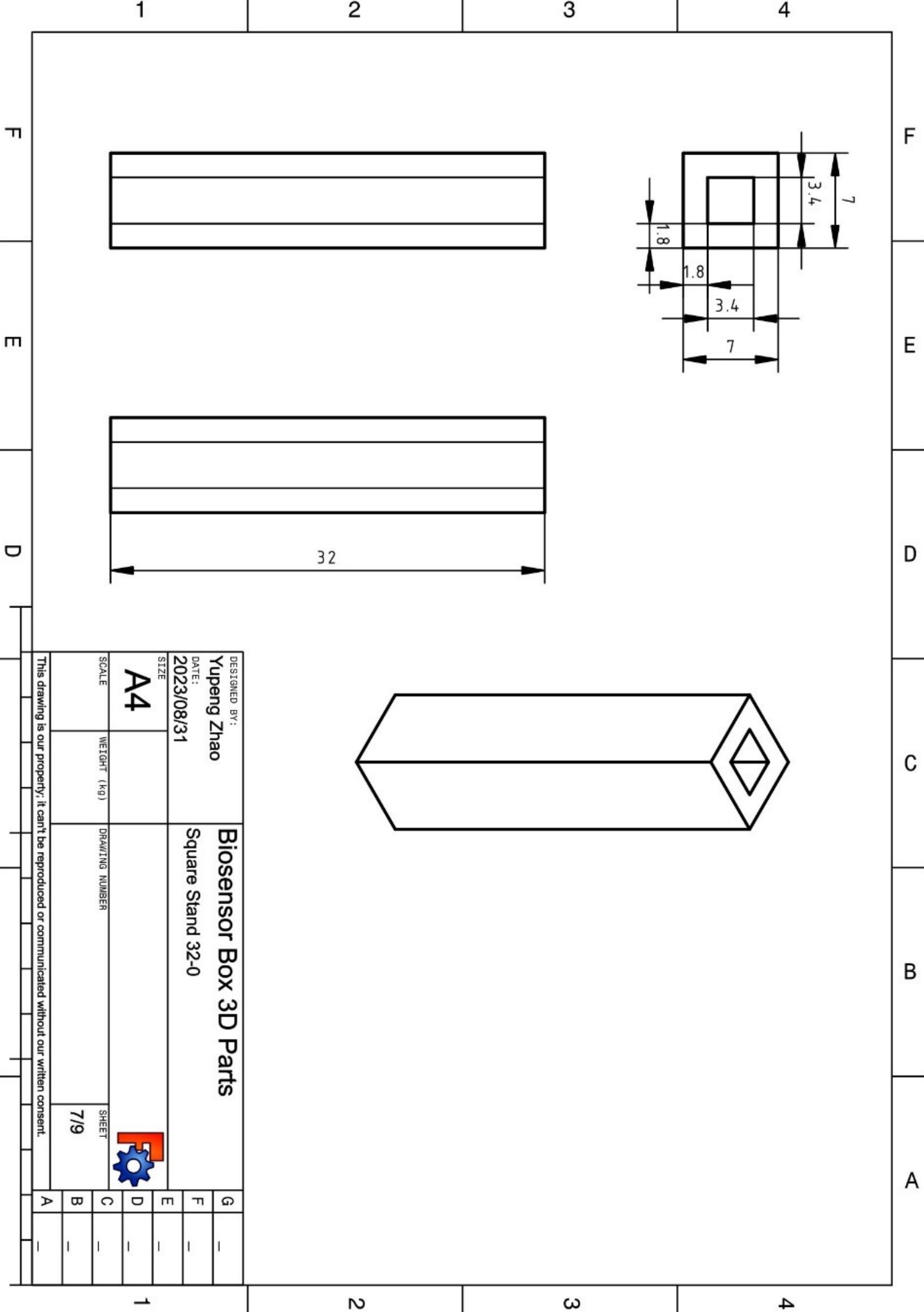


DESIGNED BY: Yupeng Zhao		Biosensor Box 3D Parts		G	-
DATE: 2023/08/31		Solid Probe Support		F	-
SIZE A4				E	-
SCALE				D	-
WEIGHT (kg)				C	-
DRAWING NUMBER				B	-
				A	-
SHEET 5/9					
This drawing is our property, it can't be reproduced or communicated without our written consent.					



DESIGNED BY: Yupeng Zhao		Biosensor Box 3D Parts	
DATE: 2023/08/31		LED Support	
SIZE A4	WEIGHT (kg)	DRAWING NUMBER	SHEET 6/9
SCALE			
This drawing is our property. It can't be reproduced or communicated without our written consent.			

Grid labels: 1, 2, 3, 4 (horizontal); F, E, D, C, B, A (vertical)

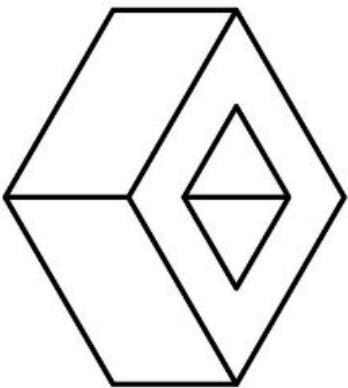
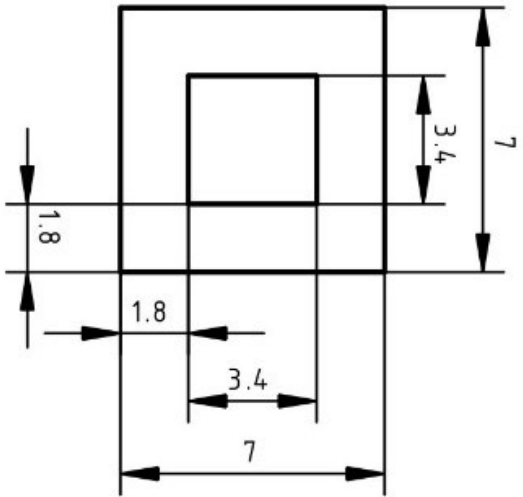


DESIGNED BY: Yupeng Zhao		Biosensor Box 3D Parts	
DATE: 2023/08/31		Square Stand 32-0	
SCALE	WEIGHT (kg)	DRAWING NUMBER	SHEET
A4			7/9



This drawing is our property. It can't be reproduced or communicated without our written consent.

G	1
F	1
E	1
D	1
C	1
B	1
A	1



DESIGNED BY:
Yupeng Zhao

DATE:
2023/08/31

Biosensor Box 3D Parts
Square Stand 4-0

SIZE
A4

SCALE

WEIGHT (kg)

DRAWING NUMBER

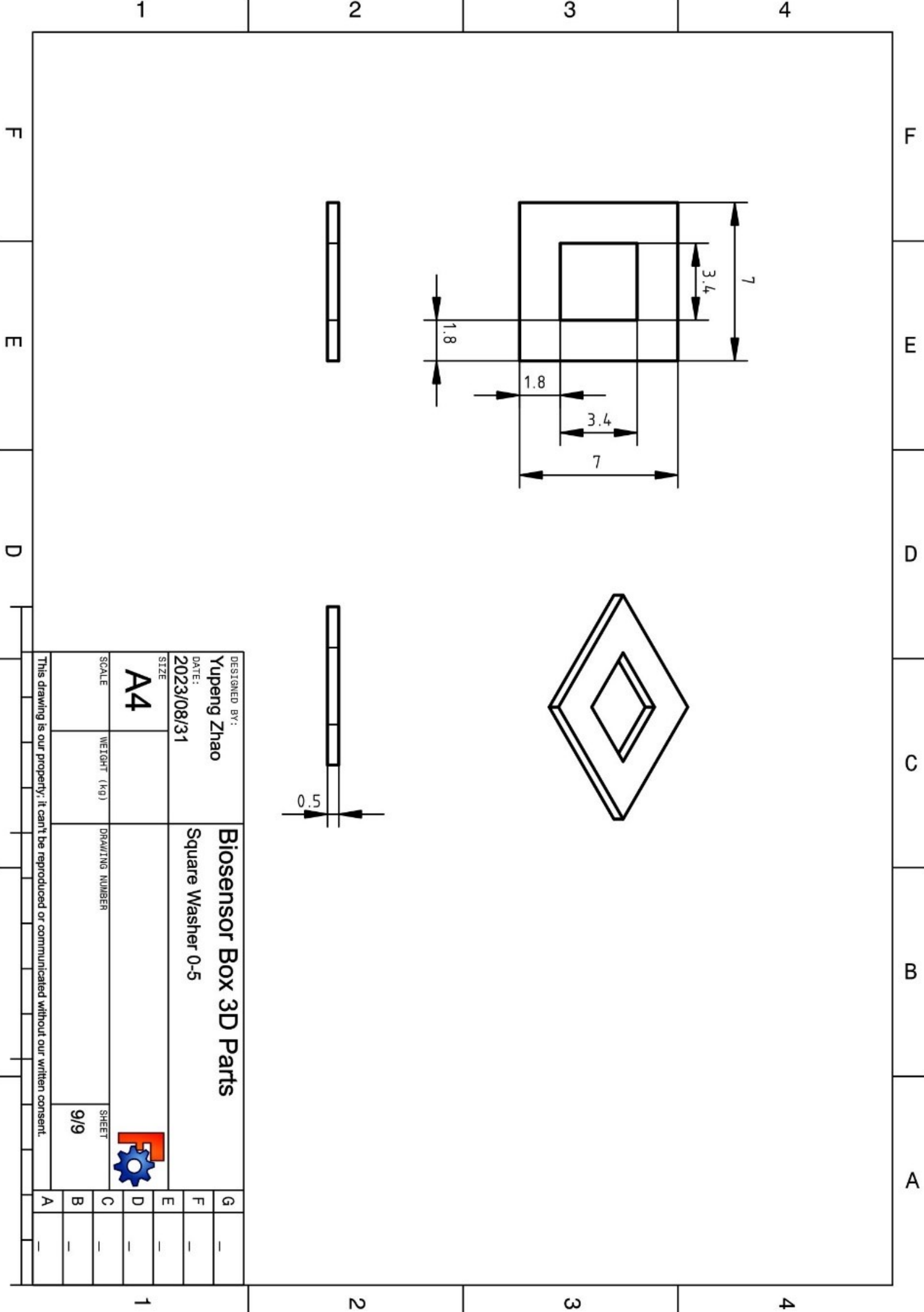
SHEET


8/9



This drawing is our property; it can't be reproduced or communicated without our written consent.

G	1
F	1
E	1
D	1
C	1
B	1
A	1



DESIGNED BY:	Yupeng Zhao			
DATE:	2023/08/31			
SIZE	A4			
SCALE		WEIGHT (kg)	DRAWING NUMBER	SHEET
				9/9
This drawing is our property. It can't be reproduced or communicated without our written consent.				

Biosensor Box 3D Parts
Square Washer 0-5

G	1
F	1
E	1
D	1
C	1
B	1
A	1

Appendix H: Tables of Collected Data

Table 8. NaCl (aq.)-silicon interface transient peak currents at three wavelengths and two intensities due to pyroelectric and photoelectric effects, collected using the Tektronix oscilloscope.

NaCl concentration (M)	Transient Peak Currents (A)					
	470 Blue 13.4 <i>mW/cm²</i>	470 Blue 6.67 <i>mW/cm²</i>	660 Red 1.72 <i>mW/cm²</i>	660 Red 0.885 <i>mW/cm²</i>	880 Infra 1.60 <i>mW/cm²</i>	880 Infra 0.564 <i>mW/cm²</i>
0	6.68E-08	6.23E-08	5.58E-08	5.23E-08	5.37E-08	5.00E-08
2.00E-12	6.22E-08	5.92E-08	5.68E-08	5.43E-08	5.75E-08	5.50E-08
2.00E-11	6.15E-08	5.95E-08	5.77E-08	5.53E-08	5.50E-08	4.92E-08
2.00E-10	6.23E-08	5.83E-08	5.87E-08	5.58E-08	5.68E-08	5.13E-08
2.00E-09	6.72E-08	6.35E-08	6.10E-08	5.78E-08	6.03E-08	5.63E-08
2.00E-08	7.18E-08	6.82E-08	6.35E-08	6.15E-08	6.18E-08	6.00E-08
2.00E-07	7.15E-08	6.77E-08	6.10E-08	5.78E-08	5.95E-08	5.63E-08
2.00E-06	7.10E-08	6.67E-08	6.07E-08	5.82E-08	5.80E-08	5.52E-08
2.00E-05	7.12E-08	6.75E-08	6.47E-08	6.12E-08	5.93E-08	5.83E-08
1.00E-04	6.95E-08	6.53E-08	6.28E-08	6.05E-08	6.20E-08	6.03E-08
1.00E-03	6.70E-08	5.95E-08	5.83E-08	5.48E-08	5.78E-08	5.40E-08
1.00E-02	5.75E-08	5.50E-08	5.13E-08	4.85E-08	4.98E-08	4.45E-08
1.00E-01	4.60E-08	4.32E-08	3.93E-08	3.60E-08	3.85E-08	3.50E-08

Table 9. NaCl (aq.)-silicon interface steady-state currents.

NaCl concentration (M)	Steady-state Currents (A)					
	470 Blue 13.4 <i>mW/cm²</i>	470 Blue 6.67 <i>mW/cm²</i>	660 Red 1.72 <i>mW/cm²</i>	660 Red 0.885 <i>mW/cm²</i>	880 Infra 1.60 <i>mW/cm²</i>	880 Infra 0.564 <i>mW/cm²</i>
0	1.42E-08	9.93E-09	5.48E-09	3.25E-09	5.68E-09	3.77E-09
2.00E-12	1.20E-08	9.63E-09	3.53E-09	3.32E-09	4.67E-09	4.42E-09
2.00E-11	9.43E-09	9.20E-09	3.25E-09	2.57E-09	4.27E-09	2.57E-09
2.00E-10	9.50E-09	7.45E-09	3.50E-09	3.03E-09	4.42E-09	3.37E-09
2.00E-09	9.07E-09	7.40E-09	3.68E-09	2.75E-09	4.57E-09	3.62E-09
2.00E-08	9.62E-09	7.70E-09	3.72E-09	3.43E-09	4.28E-09	4.27E-09
2.00E-07	9.20E-09	7.43E-09	3.80E-09	3.00E-09	4.63E-09	3.62E-09
2.00E-06	8.77E-09	6.97E-09	3.48E-09	2.83E-09	3.60E-09	3.22E-09
2.00E-05	7.93E-09	6.47E-09	3.57E-09	3.00E-09	3.30E-09	3.07E-09
1.00E-04	8.68E-09	6.45E-09	3.28E-09	2.77E-09	3.78E-09	3.60E-09
1.00E-03	6.47E-09	3.93E-09	2.60E-09	2.05E-09	3.20E-09	2.22E-09
1.00E-02	3.60E-09	2.88E-09	1.47E-09	1.31E-09	1.52E-09	1.13E-09
1.00E-01	3.18E-09	2.37E-09	1.52E-09	1.21E-09	1.62E-09	1.21E-09

Table 10. NaCl (aq.)-silicon interface transient peak currents due to pyroelectric and photoelectric effects with reverse voltage biases, collected using the biosensor box.

NaCl Concentration (M)	Transient Peak Currents (A) with Reverse Voltage Biases				
	$V_{bias} = 0 V$	$V_{bias} = -0.1 V$	$V_{bias} = -0.2 V$	$V_{bias} = -0.3 V$	$V_{bias} = -0.4 V$
0	3.45E-07	2.55E-07	1.65E-07	8.50E-08	3.50E-08
1.00E-12	2.70E-07	2.20E-07	1.55E-07	9.00E-08	4.00E-08
1.00E-11	2.95E-07	2.45E-07	2.10E-07	1.15E-07	6.00E-08
1.00E-10	3.15E-07	2.55E-07	2.20E-07	1.70E-07	1.15E-07
1.00E-09	3.50E-07	2.90E-07	2.45E-07	1.05E-07	5.00E-08
1.00E-08	3.30E-07	2.70E-07	2.30E-07	1.90E-07	5.00E-08
2.00E-08	3.55E-07	2.90E-07	2.50E-07	2.00E-07	1.35E-07
1.00E-07	6.10E-07	5.05E-07	4.25E-07	2.75E-07	1.85E-07
1.00E-06	2.75E-07	2.35E-07	1.65E-07	1.00E-07	5.00E-08
1.00E-05	3.40E-07	2.75E-07	2.35E-07	1.75E-07	8.00E-08
1.00E-04	4.05E-07	3.30E-07	2.65E-07	1.80E-07	1.05E-07
1.00E-03	6.05E-07	4.55E-07	3.00E-07	1.70E-07	7.00E-08
1.00E-02	7.30E-07	5.05E-07	2.90E-07	1.05E-07	3.50E-08
1.00E-01	4.20E-07	2.15E-07	1.05E-07	3.50E-08	1.50E-08

Table 11. NaCl (aq.)-silicon interface transient peak currents with forward voltage biases.

NaCl Concentration (M)	Transient Peak Currents (A) with Forward Voltage Biases				
	$V_{bias} = 0 V$	$V_{bias} = 0.1 V$	$V_{bias} = 0.2 V$	$V_{bias} = 0.3 V$	$V_{bias} = 0.4 V$
0	3.35E-07	3.95E-07	4.75E-07	5.65E-07	6.30E-07
1.00E-12	3.25E-07	3.90E-07	4.45E-07	5.15E-07	5.75E-07
1.00E-11	2.40E-07	2.85E-07	3.55E-07	4.15E-07	4.55E-07
1.00E-10	2.75E-07	3.35E-07	4.00E-07	4.40E-07	4.90E-07
1.00E-09	2.30E-07	2.70E-07	3.35E-07	3.95E-07	4.35E-07
1.00E-08	2.30E-07	2.75E-07	3.40E-07	3.95E-07	4.40E-07
2.00E-08	3.00E-07	3.60E-07	3.95E-07	4.70E-07	5.25E-07
1.00E-07	5.00E-07	6.00E-07	7.10E-07	8.00E-07	8.55E-07
1.00E-06	2.80E-07	3.40E-07	4.05E-07	4.65E-07	5.10E-07
1.00E-05	2.70E-07	3.20E-07	3.80E-07	4.55E-07	5.20E-07
1.00E-04	4.65E-07	5.70E-07	6.90E-07	7.85E-07	8.45E-07
1.00E-03	6.30E-07	7.40E-07	8.25E-07	9.35E-07	1.08E-06
1.00E-02	4.20E-07	6.15E-07	8.15E-07	9.60E-07	1.11E-06
1.00E-01	3.80E-07	6.85E-07	9.70E-07	1.27E-06	1.40E-06

Table 12. NaCl (aq.)-silicon interface capacitance.

NaCl concentration (M)	Interface Capacitance (nF)	Ratio with respect to 0 M
0	43	1.00
1.00E-12	58	1.35
1.00E-11	34	0.791
1.00E-10	37	0.860
1.00E-09	44	1.02
1.00E-08	45	1.05
2.00E-08	54	1.26
1.00E-07	106	2.47
1.00E-06	38	0.884
1.00E-05	52	1.21
1.00E-04	113	2.63
1.00E-03	163	3.79
1.00E-02	198	4.60
1.00E-01	152	3.53

Table 13. TNF- α cytokine-aptamer interface electric current responses due to pyroelectric and photoelectric effects, collected using the Tektronix oscilloscope.

Cytokine Concentration (M)	Transient Peak Current (A)	Steady-state Current (A)
0	5.75E-08	1.92E-08
1.00E-15	5.03E-08	1.05E-08
1.00E-14	4.95E-08	1.01E-08
1.00E-13	4.78E-08	1.12E-08
1.00E-12	5.25E-08	1.90E-08
1.00E-11	4.97E-08	2.13E-08
1.00E-10	5.03E-08	1.88E-08
1.00E-09	4.95E-08	1.78E-08
1.00E-08	4.97E-08	1.73E-08
1.00E-07	4.88E-08	1.27E-08